



This is to certify that the

dissertation entitled

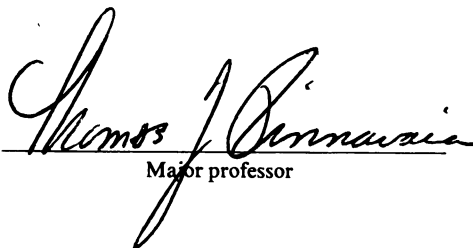
Synthesis and Catalytic Properties
of Chromia Pillared Clays

presented by

Thomas Daniel Brewer

has been accepted towards fulfillment
of the requirements for

Ph.D degree in Chemistry


Major professor

Date August 17, 1992



PLACE IN RETURN BOX to remove this checkout from your record.
TO AVOID FINES return on or before date due.

DATE DUE	DATE DUE	DATE DUE
_____	_____	_____
_____	_____	_____
_____	_____	_____
_____	_____	_____
_____	_____	_____
_____	_____	_____
_____	_____	_____

SYNTHESIS AND CATALYTIC PROPERTIES
OF CHROMIA PILLARED CLAYS

By

THOMAS DANIEL BREWER

A DISSERTATION

Submitted to
Michigan State University
in partial fulfillment of the requirements
for the degree of

DOCTOR OF PHILOSOPHY

Department of Chemistry

1992

ABSTRACT

SYNTHESIS AND CATALYTIC PROPERTIES OF CHROMIA PILLARED CLAYS

By

Thomas Daniel Brewer

Host clay layer charge and chromium pillaring solution synthesis conditions have a profound effect on the resulting physical properties of chromia pillared clays. Large gallery chromia pillared clays, with gallery heights greater than 10Å, can be obtained from smectite clay hosts of relatively low layer charge. As the host clay layer charge increases, chromia pillared clay gallery heights decrease. Surface areas in excess of 500 m²/g have been observed for chromia pillared montmorillonite after calcination at 500°C. The chromia pillared clays also show interesting thermal stabilities.

Chromia pillared clays are unique bifunctional catalysts which exhibit both acidic and redox properties. The chromia pillars, which prop the smectite clay layers apart, are the source of the catalytic activity. The vertical height and lateral spacing of the pillars define a two-dimensional nanoporous environment for possible catalytic shape selectivity. The acidic properties of chromia pillared clays have been examined using decane cracking and a standard gas oil microactivity test as probe reactions. In addition, since chromia is a known

Thomas Daniel Brewer

dehydrocyclization catalyst, the aromatization of n-octane to p-xylene has been used to study the redox and shape selective properties. While chromia pillared clays do not exhibit exceptional shape selectivity for the n-octane dehydrocyclization reaction, a pore effect on the product distribution has been observed when compared to that of a non-microporous chromia on alumina catalyst.

The hydroconversion of n-heptane over a chromia pillared montmorillonite catalyst and an alumina pillared montmorillonite catalyst are also compared. The yield of cracked products closely followed the conversion for the chromia pillared clay catalyst, while the formation of isomerized products was dependent upon the pretreatment temperature in air.

To My Family

ACKNOWLEDGMENTS

I would like to thank Dr. T.J. Pinnavaia for preparing me to survive in the outside world. His "sink or swim" philosophy has made me a good swimmer in the turbulent waters of the industrial world. I also appreciate his understanding of the difficult time I went through after I secured employment before completing my dissertation.

I would also like to thank Koch Industries for letting me use their library to obtain numerous references. It was a result of their corporate reorganization that catalyzed my self evaluation and realization that many of my decisions were preventing me from succeeding in life. My difficult experience has allowed me to grow and mature in a unique way; however, I don't recommend that any student leave graduate school before completing all the requirements for a degree.

Lastly, I would like to thank my family, friends, and committee members who have waited patiently for years to see me finish this dissertation.

TABLE OF CONTENTS

	<u>PAGE</u>
LIST OF TABLES.....	viii
LIST OF FIGURES.....	ix
CHAPTER I - INTRODUCTION.....	1
Clays.....	1
Catalysis.....	5
CHAPTER II - CHROMIA PILLARED CLAYS.....	9
INTRODUCTION.....	9
EXPERIMENTAL.....	11
Materials.....	11
Pillaring Reactions.....	12
Physical Methods.....	13
Chemical Analysis.....	14
Cation Exchange Capacity (CEC).....	14
Electron Microscopy.....	15
RESULTS AND DISCUSSION.....	16
Chromia Pillared Montmorillonite (CPM).....	16
Effect of Clay Layer Charge.....	26
REFERENCES.....	41
CHAPTER III - CATALYTIC PROPERTIES OF CHROMIA PILLARED CLAYS.....	44
INTRODUCTION.....	44

	<u>PAGE</u>
EXPERIMENTAL.....	47
Materials.....	47
Pillaring Reactions.....	48
Physical Methods.....	50
Catalytic Methods.....	52
RESULTS.....	55
Acidity.....	55
Cracking Reactions.....	58
Octane Aromatization.....	62
DISCUSSION.....	72
REFERENCES.....	83
CHAPTER IV - CHROMIA AND ALUMINA PILLARED MONTMORILLONITE CATALYZED HYDROCONVERSION OF N-HEPTANE.....	86
INTRODUCTION.....	86
EXPERIMENTAL.....	88
Chromial Pillared Montmorillonite.....	88
Alumina Pillared Montmorillonite.....	88
Physical Methods.....	89
RESULTS AND DISCUSSION.....	91
Physical Characterization.....	91
Hydroconversion of n-heptane.....	91
REFERENCES.....	99

LIST OF TABLES

<u>Table</u>	<u>Page</u>
1	Idealized structural formulas for some 2:1 clay minerals.....4
2	Basic properties of smectite clays.....6
3	Effect of OH/Cr ratio in pillaring solution on resulting CPM x-ray basal spacing and surface area.....19
4	Physical properties of CPM resulting from room temperature and elevated temperature chromium hydrolysis.....22
5	Physical properties of chromia pillared smectites.....37
6	MAT results for gas oil cracking over chromia pillared montmorillonite and alumina pillared montmorillonite (APM).....59
7	Decane cracking product distributions of CPM, CPH, and a commercial chromia on alumina catalyst.....61
8	Aromatization of n-octane over CPM, CPH, and a commercial chromia on alumina catalyst...63
9	Effect of catalyst prereduction on n-octane aromatization.....66
10	Physical properties of APM and CPM.....92

LIST OF FIGURES

<u>Figure</u>	<u>Page</u>
1	Unit-structure of a 2:1 layer-type clay.....2
2	Idealized representation of a pillared clay.....7
3	XRD patterns of CPM products after dehydroxylation at 350°C under nitrogen for 2 hours: A. Product obtained by aging pillaring solution 36 hrs at 100°C with OH/Cr=2.0. B. Product obtained by aging pillaring solution 36 hrs at 25°C with OH/Cr=2.0.....17
4	Q-Plot of CPM.....20
5	TEM electron micrograph of CPM with $d_{001}=21.5\text{\AA}$, magnification=385,000X.....23
6	Temperature dependent XRD patterns of CPM. Pillaring solution aged at 100°C for 36 hours, OH/Cr=2.0.....25
7	XRD patterns (350°C) of chromia pillared hectorite (CPH), montmorillonite (CPM), beidellite (CPB), and fluorohectorite (CPF), along with the host clay cation exchange capacity in meq/100g.....27
8	TEM electron micrograph of chromia pillared beidellite (CPB) with $d_{001}=16.5\text{\AA}$, magnification=525,000X.....29
9	XRD patterns of CPM (350°C) prepared by: A. Direct Exchange and B. In situ hydrolysis of the chromia pillaring solution. Pillaring solution aged at 100°C for 36 hours, OH/Cr=2.0.....32
10	XRD patterns (350°C) of 0-30% RCCPM. Pillaring solution aged at 100°C for 36 hours, OH/Cr=2.0.....35

<u>Figure</u>		<u>Page</u>
11	One possible structure of the trinuclear aqua chromium (III) cation, $\text{Cr}_3(\text{OH})_4(\text{H}_2\text{O})_9^{5+}$	40
12	Schematic diagram of the continuous flow microreactor used for catalyst testing.....	53
13	Temperature dependent acidity of chromia pillared clay (DE-CPM) as measured by pyridine adsorption.....	56
14	Temperature dependent FTIR spectra of pyridine adsorbed on DE-CPM. L: Lewis bound pyridine, B: Bronsted bound pyridine. Spectra were recorded at the temperature shown.....	57
15	Octane aromatization selectivity versus time for DE-CPM catalyst with/without prereduction.....	65
16	Octane aromatization selectivity to o- xylene with time over various chromia catalysts.....	68
17	Octane aromatization selectivity to m- xylene with time over various chromia catalysts.....	70
18	Octane aromatization selectivity to p- xylene with time over various chromia catalysts.....	71
19	Temperature-programmed hydroconversion of n-heptane over CPM. Catalyst pretreatment: 2 hrs at 400°C in air, H ₂	93
20	Temperature-programmed hydroconversion of n-heptane over CPM. Catalyst pretreatment: 2 hrs at 250°C in air, H ₂	94
21	Temperature-programmed hydroconversion of n-heptane over CPM and APM.....	96
22	Percentage of C ₇ isomers in the reaction products as a function of reaction temperature for the temperature-programmed hydroconversion of n-heptane over CPM and APM.....	97

CHAPTER I

INTRODUCTION

Clays

Clays and clay minerals are fine textured, layered hydrous phyllosilicates, typically with diameters less than 2 microns. The basic configuration of the clay layer-structure consists of planes, sheets, layers, and interlayers. A single plane of atoms or ions is the minimum unit, while a sheet is composed of a combination of planes. A clay layer is made up of a combination of sheets. Layers are often separated from one another by an interlayer region.

Figure 1 depicts the unit-structure of a 2:1 layer-type clay, which will be the only layer type used in this study. Each layer is composed of 4 planes of oxygen and hydroxyl atoms and ions, which are arranged to form two tetrahedral sheets above and below an octahedral sheet, i.e. 2 tetrahedral sheets : 1 octahedral sheet. One can visualize the sheets by considering the tetrahedra as being corner shared and the octahedra as being edge shared. Between each layer is the interlayer, or gallery, region, which is typically occupied by hydrated alkali or alkaline earth cations.

The clays used in this study contain varying degrees of negative layer charge, which is compensated for in the interlayer with cations. The source of the negative layer charge is isomorphous substitution of cations with a lower valence than the typical cations found in the tetrahedral and/or octahedral vacancies, which are defined by the clay sheets. If the amount of substitution is large, then the interaction between the clay layers and the interlayer cations is strong, and the interlayer cations will be difficult to exchange. Interlayer cation exchange is necessary to separate the clay layers and change the physicochemical properties of these materials. If the amount of substitution is small or zero, then the clay layers will be in van der Waals contact, and will again be difficult to separate. However, if the amount of layer cation isomorphous substitution is of an intermediate value, then the layer charge will also be intermediate, and the clay will be able to be cation exchanged.

Table 1 shows some idealized structural formulas for a few clay minerals listed in order of increasing layer charge density; from no layer charge to a large layer charge. The two subdivisions, dioctahedral and trioctahedral, refer to whether two-thirds (di) or three-thirds (tri) of the octahedral cation vacancies are occupied. Dioctahedral clays contain primarily valence three cations in the octahedral vacancies, while trioctahedral clays contain primarily valence two cations in the octahedral vacancies.

Table 1: Idealized structural formulas for some 2:1 clay minerals.

Diocahedral
Pyrophyllite: $[\text{Al}_{4.0}](\text{Si}_{8.0})\text{O}_{20}(\text{OH})_4$
Montmorillonite: $\text{M}_{x/n}^{n+} \cdot y\text{H}_2\text{O}[\text{Al}_{4.0-x}\text{Mg}_x](\text{Si}_{8.0})\text{O}_{20}(\text{OH})_4$
Beidellite: $\text{M}_{x/n}^{n+} \cdot y\text{H}_2\text{O}[\text{Al}_{4.0}](\text{Si}_{8.0-x}\text{Al}_x)\text{O}_{20}(\text{OH})_4$
Nontronite: $\text{M}_{x/n}^{n+} \cdot y\text{H}_2\text{O}[\text{Fe}_{4.0}](\text{Si}_{8.0-x}\text{Al}_x)\text{O}_{20}(\text{OH})_4$
Muscovite: $\text{K}_2[\text{Al}_{4.0}](\text{Si}_{6.0}\text{Al}_{2.0})\text{O}_{20}(\text{OH})_4$
Triocahedral
Talc: $[\text{Mg}_{6.0}](\text{Si}_{8.0})\text{O}_{20}(\text{OH})_4$
Hectorite: $\text{M}_{x/n}^{n+} \cdot y\text{H}_2\text{O}[\text{Mg}_{6.0-x}\text{Li}_x](\text{Si}_{8.0})\text{O}_{20}(\text{OH},\text{F})_4^*$
Saponite: $\text{M}_{x/n}^{n+} \cdot y\text{H}_2\text{O}[\text{Mg}_{6.0}](\text{Si}_{8.0-x}\text{Al}_x)\text{O}_{20}(\text{OH})_4$
Phlogopite: $\text{K}_2[\text{Mg}_{6.0}](\text{Si}_{6.0}\text{Al}_{2.0})\text{O}_{20}(\text{OH})_4$



Clays such as montmorillonite, beidellite, and hectorite contain an intermediate amount of layer charge and can be swelled (layers expanded) in an appropriate solvent. Table 2 lists some basic properties of swelling, or smectite, clays.

One can utilize the chemistry of swelling clays by exchanging the initial interlayer cations with large polyoxocations. Such large cations can then serve to prop the clay layers apart in a permanent manner after dehydration/dehydroxylation. If there is also lateral spacing between the clay layer props, the clay is said to be pillared, as represented in Figure 2.

Catalysis

There are three major catalyst markets -- petroleum refining, chemical processing, and emissions control. Research in all areas concern the development of products with improved performance to meet changing environmental standards and considerations. For example, refiners need catalysts to meet the production requirements of reformulated gasoline, and the automotive, process, and energy industries need catalysts to reduce emissions.

The current worldwide merchant catalyst market is nearly \$6 billion. The worldwide market for catalysts is predicted to grow about 4% per year during the next few years, according to Catalyst Group, a Spring House, Pa.-based consulting firm. The petroleum refining catalyst



Table 2: Basic properties of smectite clays.

A) Cation Exchangers (60-120 meq/100g)

- 1) Simple hydrated cations
- 2) Mono-polynuclear complexes
- 3) Onium ions
- 4) Carbocations

B) Swellable

- 1) Multilayers of guests between host layers
- 2) Gallery heights range from zero to infinity
- 3) Dependent upon layer charge, exchange ion, solvent

C) High Intercrystalline Surface Area

- 1) Typically 750 m²/g
- 2) Some lost due to stacking

D) Colloidal Particles

- 1) Typically less than 2 microns



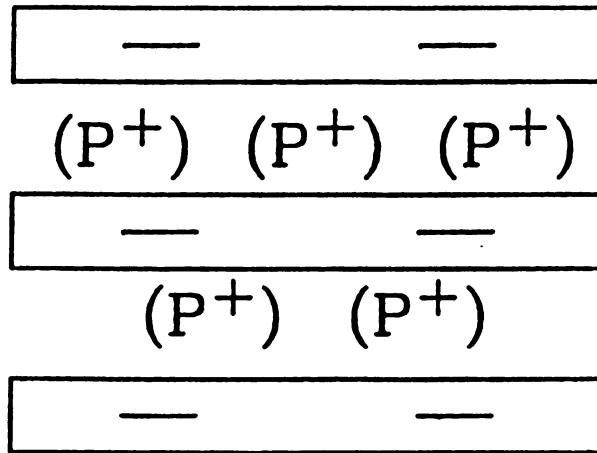


Figure 2: Idealized representation of a pillared clay.

market, which includes fluid cracking catalysts (FCC), hydrocracking, reforming, isomerization, hydrotreating, and alkylation, is undergoing the greatest amount of change.

It is clearly evident that there is a large potential for novel catalytic materials to be utilized in the solution of today's catalytic challenges. Pillared clays composed of pillaring species which are active catalytic centers, such as chromia, are novel catalytic materials which can act as bifunctional, acid and redox, catalysts. The objective of this dissertation research was to prepare very large gallery height chromia pillared clays, and to study the resulting catalytic properties of these materials.

CHAPTER II

CHROMIA PILLARED CLAYS

INTRODUCTION

Super gallery pillared clays are a new class of pillared materials with exceptionally large gallery heights ($>20\text{\AA}$). Recent work shows that the direct intercalation of metal oxide sol particles (DIMOS) is one rational approach to the synthesis of these highly expanded materials(1-2). Metal oxide pillared clays typically are formed by the direct intercalation of robust polyoxocations between the negatively charged clay layers(3-5). The intercalated polyoxocations are then thermally dehydrated/dehydroxylated, which converts the cations into molecular-sized oxide aggregates (pillars) with gallery heights ranging from 0.4 to 2 times the 9.6\AA van der Waals thickness of the host clay layer(6-13). These metal oxide pillared clays show novel microporosity(14-15) as well as interesting catalytic properties(16-21).

Chromia pillared montmorillonite (CPM) was first synthesized in 1979 by the intercalation of base hydrolyzed chromium nitrate solutions(22). Hydroxy chromium

interlayered clays were also studied by Rengasamy and Oades, who found that the adsorption of chromium cations on clay surfaces was related to pH(23). In addition to the extensive, but slow, hydrolysis chemistry observed for Cr^{3+} cations in aqueous solution(24), further hydrolysis has been reported to occur in the clay galleries(22,25-26). Very large basal spacings ($d_{001}=21\text{-}28\text{\AA}$) have been observed for chromia pillared montmorillonite using an elevated hydrolysis temperature and Na_2CO_3 as the source of base during the chromium hydrolysis reaction (27-28). We now report the synthesis of other chromia pillared smectites, each showing unique basal spacings. The ability to synthesize pillared smectites with large basal spacings is dependent upon both the preparation of large chromium polyoxocations and the host clay layer charge.

EXPERIMENTAL

Materials

Wyoming montmorillonite (SWy-1) was obtained from Source Clay Minerals Repository at the University of Missouri, Columbia, Mo. Montmorillonite was further purified by preparing a two weight percent aqueous suspension to sediment overnight to obtain the size fraction consisting of less than or equal to 2 micron particles. The clay fraction was then sodium exchanged by mixing with a 20-fold excess of NaCl at room temperature for one hour. The clay was then dialyzed until a negative silver nitrate test was obtained for chloride ion. Chemical analysis of the resulting purified Na-montmorillonite indicated a unit cell formula of $\text{Na}_{0.66}[\text{Al}_{3.12}\text{Fe}_{0.40}\text{Mg}_{0.48}](\text{Si}_{7.82}\text{Al}_{0.18})\text{O}_{20}(\text{OH})_4$.

Na-beidellite, of structural formula $\text{Na}_{0.90}[\text{Al}_{4.00}](\text{Si}_{7.10}\text{Al}_{0.90})\text{O}_{20}(\text{OH})_4$, was provided by George Poncelet from the Université Catholique de Louvain.

Ca-hectorite was obtained by the Source Clay Minerals Repository (SHCa-1), and was further purified and sodium exchanged using the same procedure as that for montmorillonite. The unit cell formula for purified Na-hectorite was $\text{Na}_{0.62}[\text{Mg}_{5.38}\text{Li}_{0.62}](\text{Si}_{8.00})\text{O}_{20}(\text{OH})_4$.

The synthetic Li-fluorhectorite used in this work had a unit cell formula of $\text{Li}_{1.24}[\text{Mg}_{4.76}\text{Li}_{1.24}](\text{Si}_{8.00})\text{O}_{20}(\text{OH})_4$.



Pillaring Reactions

Chromia pillared smectites were prepared similar to a previously published procedure (27). In order to pillar one gram of purified Na-montmorillonite, a 0.25M aqueous Na_2CO_3 solution was added dropwise to 0.05 mole $\text{Cr}(\text{NO}_3)_3$ (60 moles of chromium per clay exchange equivalent) until the final Cr concentration was 0.10M and the desired OH/Cr ratio was achieved. The pillaring solution was allowed to age for 36 hours at either room temperature or 100°C , after which a 1 wt % aqueous clay suspension was added and the resulting mixture stirred for 1.5 hours. The chromium exchanged clay was washed free of excess salt by repeated centrifugation/dispersion cycles until flocculated particles were present. The product, at 1 wt %, was air dried on a glass sheet. The resulting film was peeled, dehydrated/dehydroxlated at 350°C under inert gas (nitrogen or argon), ground in a mortar and pestle and sieved to a particle size of 250-500 microns.

A series of reduced charge montmorillonite (RCM) samples were prepared by the method of Brindley and Ertem (29). One wt % aqueous suspensions of Li- and Na-montmorillonite were mixed in the following proportions to achieve the desired levels of charge reduction: 100:0, 90:10, 80:20, 70:30. The suspensions were stirred for 24 hours to allow randomization of the ions and then air dried on glass sheets. The resulting films were peeled and heated for 24 hours at 220°C in an oven to achieve layer charge

reduction by migration of Li^+ to empty octahedral sites in the layer. The RCM samples were then suspended in water at 1 wt % and dispersed in a blender.

Aqueous suspensions (1.0 wt %) of Na-beidellite, Na-hectorite, Li-fluorohectorite, and Na,Li-RCM were chromium exchanged and pillared following the procedure given for Na-montmorillonite. In each case, the amount of $\text{Cr}(\text{NO}_3)_3$ used per gram of smectite was adjusted such that the moles of chromium per clay exchange equivalent was 60. The pillaring solution consisted of a OH/Cr ratio of 2.0 and was aged at 100°C for 36 hours.

Physical Methods

X-ray diffraction patterns were obtained using a Rigaku rotating anode x-ray diffractometer equipped with CuK alpha radiation. Oriented thin film samples were prepared for x-ray analysis by air drying on a glass slide approximately 1 ml of a 1 wt.% freshly prepared pillared clay aqueous suspension. The slides were either analyzed at 25°C or heated to the desired temperature (100, 350, or 500°C) under inert gas for 2 hours.

Nitrogen adsorption/desorption isotherms were obtained at -196°C with either a Quantachrome Autosorb or a Quantasorb Jr. sorption analyzer using ultra high purity N_2 gas as the adsorbate and He as the reference or carrier. Approximately 100 mg samples were outgassed at 350°C under vacuum for 12 hours prior to analysis.

Chemical Analysis

Elemental analysis of the host smectites were performed on a Jarrell-Ash 955 Atom-Comp ICP-AES. Clay samples (0.05 g) were prepared for analysis by fusion with lithium borate (0.3 g, Aldrich, Gold Label) in graphite crucibles at 1000°C for 12 minutes. The resultant glass was transferred to 100 ml of 5% HNO₃ and mixed until completely dissolved. NIST plastic clay 98a served as a standard. Galbraith Laboratories, Inc. analyzed chromium pillared clay samples for Si, Al, Mg, and Cr, from which intercalated Cr per O₂₀(OH)₄ unit was calculated based on the assumption that the Si content of the host clay remained constant throughout the pillaring reaction.

Cation Exchange Capacity (CEC)

Cation exchange capacities for the host smectites were calculated by both the structural formula from total elemental analysis and by use of an ammonia electrode (30). The ammonia electrode procedure involves suspending 100 mg of ammonium-saturated clay in 40 ml H₂O made alkaline with the addition of 0.5 ml 10M NaOH. An ammonia electrode was then used to read the potential developed. The ammonium concentration was calculated by comparison with three standard ammonium solutions (10⁻², 10⁻³, and 10⁻⁴M).

Electron Microscopy

TEM observation was carried out using a JEOL 200FX microscope operating at 200 keV. The instrument is part of the University of Michigan Electron Microbeam Analysis Laboratory. Holey carbon films mounted on copper grids were dipped in the powdered specimen, which allowed only those particles small enough to remain on the grid by van der Waals force to be imaged.

RESULTS AND DISCUSSION

Chromia Pillared Montmorillonite (CPM)

The use of an aqueous solution of Na_2CO_3 , as opposed to solid Na_2CO_3 or NaOH , as a base source for the hydrolysis of the chromium pillaring solution helps minimize high localized concentrations of hydroxide ion which lead to $\text{Cr}(\text{OH})_3$ precipitation (27). The subsequent slow dissolution of the hydroxide precipitate limits the chromium concentration necessary for large polyoxocation growth. More important than the choice of base, however, is the use of vigorous aging conditions, such as elevated temperature and prolonged aging time, as well as the optimum OH/Cr ratio, to hydrolyze the Cr^{3+} cations (31).

The effect of hydrolysis temperature can be seen in Figure 3, which compares the CPM basal spacings (after 350°C dehydration/dehydroxylation) resulting from Cr pillaring solutions, $\text{OH}/\text{Cr}=2$, aged for 36 hours at either room temperature or 100°C . Room temperature Cr hydrolysis produced much smaller Cr oligomeric cations, as can be seen by the 12.3\AA basal spacing of the resulting CPM. However, elevated temperature Cr hydrolysis for the same time period produced much larger Cr polyoxocations, which after intercalation and dehydration/dehydroxylation, resulted in a chromia pillared montmorillonite with a 21.5\AA basal spacing. The peak corresponding to the 42.1\AA basal spacing is due to a nucleation controlled chromia phase which is difficult

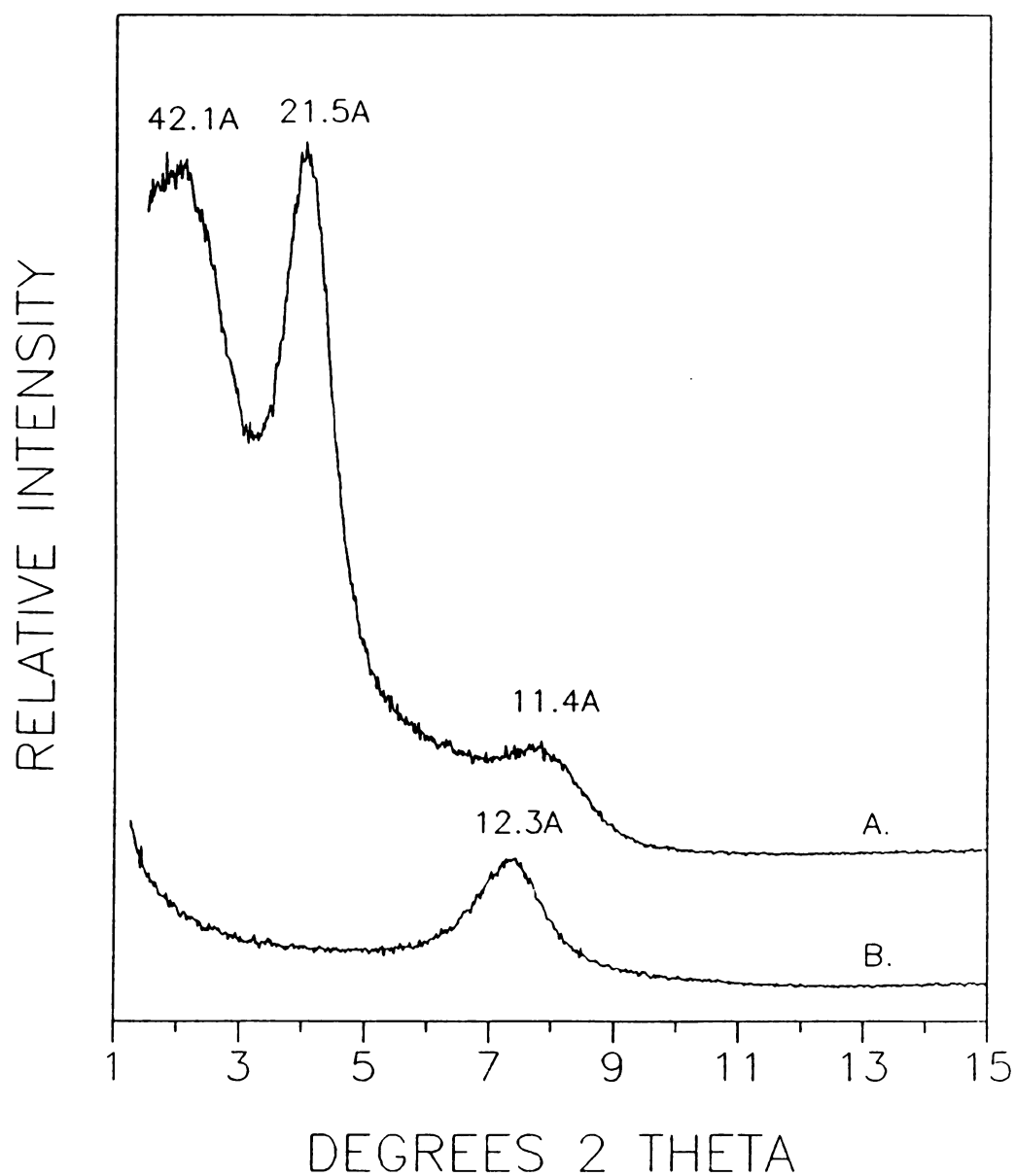


Figure 3. XRD patterns of CPM products after dehydroxylation at 350°C under nitrogen for 2 hours:

- A. Product obtained by aging pillaring solution 36 hrs at 100°C with OH/Cr=2.0
- B. Product obtained by aging pillaring solution 36 hrs at 25°C with OH/Cr=2.0

to reproduce.

Tzou (28) also observed an increase in CPM basal spacings resulting from pillaring solutions hydrolyzed at increasing temperatures and aging times. He observed a maximum, though, when the pillaring solution was aged for 36 hours at 100°C.

We observed that OH/Cr ratios greater than 1 result in faster and more extensive Cr^{3+} hydrolysis, as long as the ratio is less than 3, where $\text{Cr}(\text{OH})_3$ precipitation occurs. Table 3 shows the optimum OH/Cr ratio for large CPM basal spacings and high BET surface areas to be two. The larger OH/Cr ratio of 2.5 probably effects intermolecular hydrogen bond formation during chromium hydrolysis, which may influence the stability of polyoxocation growth (31).

The CPM containing the 42.1Å phase shows the first, second and fourth order x-ray diffractions, being more ordered than the smaller, room temperature hydrolyzed CPM, which only shows one order of diffraction. The q-plot in Figure 4 confirms that the third order diffraction is missing for this sample, as can be seen by the loss of linearity if the fourth order peak was considered to be third order. Since the methods used to obtain this chromia pillared montmorillonite with such a large d_{001} basal spacing are not unlike those used by Pinnavaia et al (27), which contains the same d_{002} and d_{004} basal spacings, it is likely that these previous x-ray diffractograms of chromia pillared montmorillonite contained similar super galleries.

Table 3. Effect of OH/Cr ratio in pillaring solution^(a) on resulting CPM x-ray basal spacing and surface area.

OH/Cr	XRD Basal Spacing (Å)		Surface Area ^(b) (m ² /g)
	25°C	350°C	
1.0	17.0	15.8	141
2.0	55.2, 26.7	42.1, 21.5	378
2.5	50.2, 25.1	40.0, 20.0	319

(a) Pillaring solution aged at 100°C for 36 hours.

(b) Surface areas determined by the BET method using nitrogen as the adsorbate.

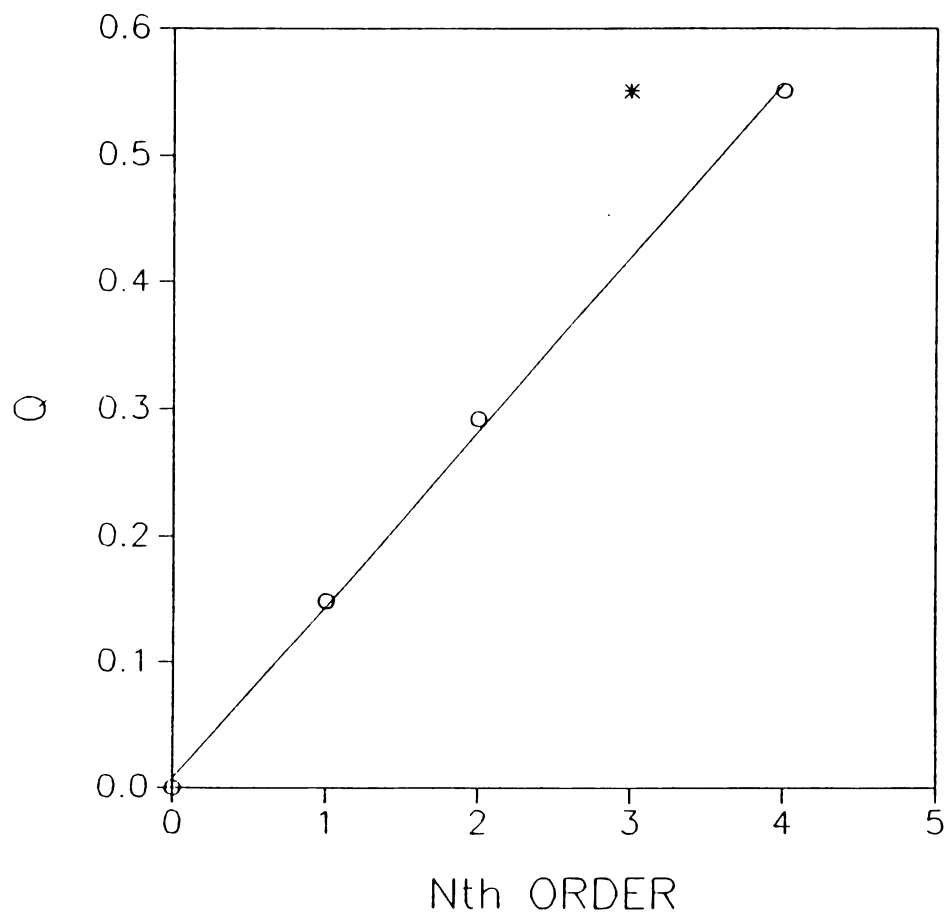


Figure 4. Q-Plot of CPM.

The CPM resulting from elevated temperature chromium hydrolysis also has a much larger BET surface area than the smaller, room temperature hydrolyzed, chromia pillared clay, 378 vs 110 m²/g (Table 4). The larger chromium polyoxocations allow for a much greater surface for the small N₂ molecules to adsorb onto. In addition, the surface areas of chromia pillared clays will appear lower than that for pillared clays with pillars composed of atoms of molecular weight similar to silicon or aluminum. Chemical analysis revealed the moles of intercalated Cr per O₂₀(OH)₄ clay unit for elevated temperature hydrolyzed CPM to be almost four times that for room temperature hydrolyzed CPM, 4.36 vs 1.14.

The broadness of the x-ray diffraction peaks can be attributed to the range of polyoxocation nuclearities (cation size) present in the Cr pillaring solution, as well as the fact that the clay layers are not perfectly rigid (32). Broad peaks can also be a result of regular interstratification, or staging, such as that observed by Singh and Kodama of a 28Å complex with a regularly interstratified structure which resulted from the reaction of polynuclear hydroxyaluminum cations with montmorillonite (33).

The electron micrograph in Figure 5 of a CPM sample shows the effect of the large chromium polyoxocations (dark spheres) on the montmorillonite layers (light wavy lines). The montmorillonite layers are not rigid enough to maintain

Table 4. Physical properties of CPM resulting from room temperature and elevated temperature chromium hydrolysis^(a).

Hydrolysis Temp. (°C)	Basal Spacing (Å)		Surface Area ^(b) (m ² /g)	Cr per unit cell
	25°C	350°C		
25	15.8	12.3	110	1.14
100	55.2, 26.7	42.1, 21.5	378	4.36

(a) OH/Cr=2.0.

(b) Surface areas determined by the BET method using nitrogen as the adsorbate.



Figure 5. TEM electron micrograph of CPM with $d_{001}=21.5\text{\AA}$, magnification=385,000X.



the large layer separation imposed by the intercalated cation. The height of the pillars (and also of the clay layers) as measured from the electron micrograph are slightly smaller than that shown by x-ray diffraction. This phenomenon has been observed before for pillared clays (34) and could be due to electron beam degradation of the specimen. However, it appears that all of the montmorillonite layers are regularly intercalated with large chromium polyoxocations, excluding the possibility of the large x-ray basal spacing being due to regular interstratification. In addition, only trace levels of Na were detected during elemental analysis of all CPM samples, and an x-ray diffraction peak at 9.6\AA is absent.

Chromia pillared montmorillonites also possess interesting thermal stabilities (Figure 6). Temperature dependent x-ray diffraction patterns show a very large 26.7\AA basal spacing at room temperature (before dehydration/dehydroxylation), with a steady decrease to 20.1\AA after a 500°C thermal treatment under inert gas. After a 500°C thermal treatment, the clay loses much of its crystallinity, most likely due to thermal migration of the pillars. In addition, the nucleation dependent chromia phase responsible for the very large gallery heights appears to be the least thermally stable. Pillar migration and decomposition can also explain the increase in surface area after thermal treatment as being due to an increase in larger micropores.

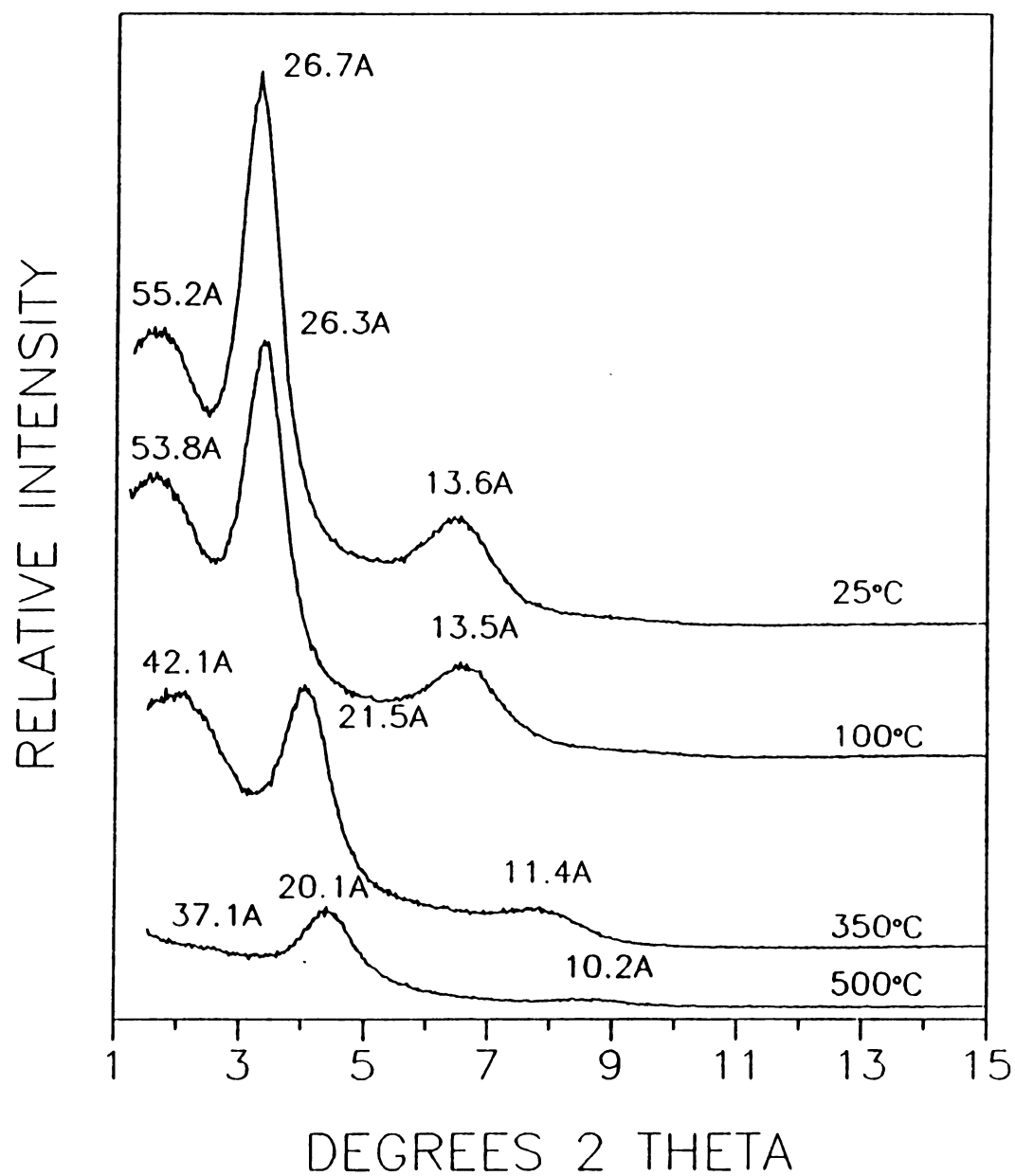


Figure 6 Temperature dependent XRD patterns of CPM. Pillaring solution aged at 100°C for 36 hours, OH/Cr=2.0.

One can also notice that the intensity of the most intense peak decreases with increasing dehydration/dehydroxylation temperature, while the intensity of the first peak does not. This would lead one to believe that there are two phases of chromium oxide composing the pillars, and that the first two x-ray diffraction peaks are not related. However, the diffraction peaks may be related, in that the centroids of the first two peaks in each diffractogram shift to larger degrees 2θ with increasing treatment temperature, and the corresponding d-spacings maintain a 2:1 ratio, as seen in the q-plot of Figure 2. Also, varying the Cr/clay ratio from 60 down to 15 had no effect on peak intensities (Cr/clay ratios less than 15 resulted in incomplete intercalation). Therefore, it is likely that we are observing both two phases of chromia in addition to the second order peak of the larger phase.

Effect of Clay Layer Charge

Other smectite hosts were chromia pillared, using the optimized conditions for preparing CPM, to determine the effect layer charge had on the physical properties of the resulting pillared clay. One smectite of lower layer charge than montmorillonite, along with two smectites of higher layer charge, were selected for pillaring by chromium. The x-ray diffraction patterns of the four chromia pillared smectites are shown in Figure 7.



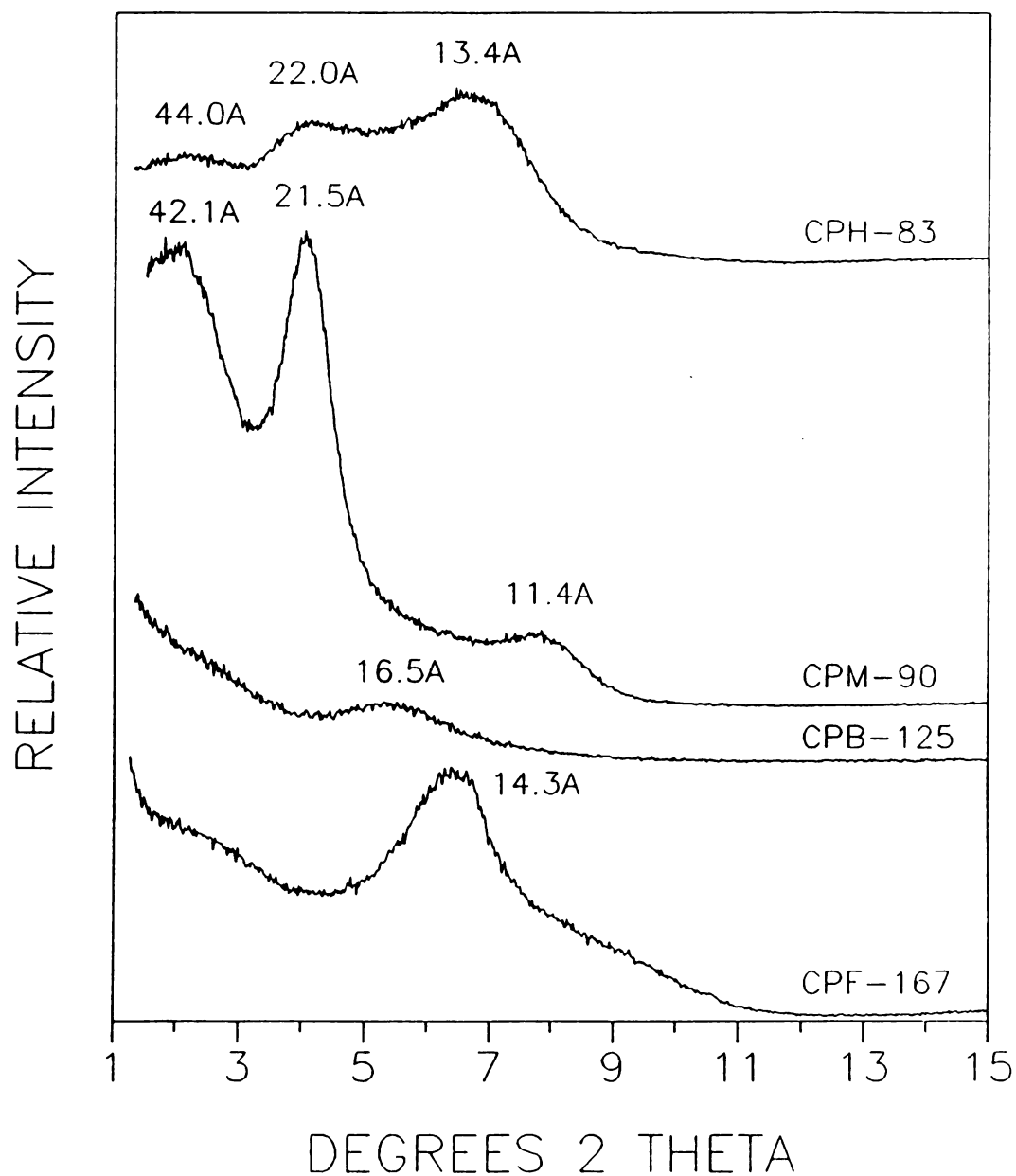


Figure 7. XRD patterns (350°C) of chromia pillared hectorite (CPH), montmorillonite (CPM), beidellite (CPB), and fluorohectorite (CPF), along with the host clay cation exchange capacity in meq/100g.

Hectorite, which has a lower cation exchange capacity than montmorillonite, 83 vs 90 meq/100g, resulted in a slightly larger expanded final pillared product than CPM. Beidellite and fluorohectorite, each having a larger cation exchange capacity than montmorillonite, 125 and 167 meq/100g, resulted in products with smaller basal spacings. The chromia pillared hectorite (CPH) also shows the first three orders of d_{001} x-ray diffraction, while the chromia pillared beidellite (CPB) and chromia pillared fluorohectorite (CPF) show only one order of diffraction. However, at small angles 2θ , the x-ray diffraction patterns for both CPB and CPF show a very weak, but discernible, broad peak. This is most likely due to the minimal presence in the gallery of chromium polyoxocations of higher nuclearity than those responsible for the smaller basal spacings.

Similar studies comparing alumina pillared montmorillonite with other smectites of higher and lower layer charge resulted in essentially no difference in the observed basal spacings (35-36). Thus, the effect of clay layer charge on chromia pillared smectite basal spacings is unique, and is not observed for other metal oxide pillared smectites. The preparation conditions of the pillar precursors, however, strongly effect all the various metal oxide pillared clay basal spacings.

The electron micrograph of CPB in Figure 8 confirms both the smaller gallery height than CPM, gallery heights

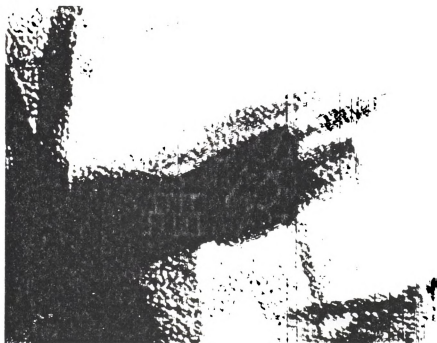
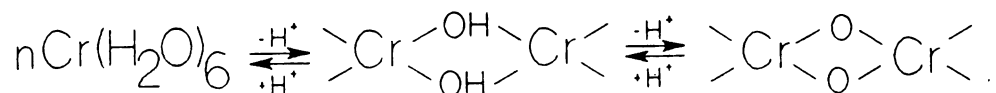


Figure 8. TEM electron micrograph of chromia pillared
beidellite (CPB) with $d_{001}=16.5\text{\AA}$
magnification=525,000X.

close to one half the thickness of the host clay layer, and the lack of interstratification. One can also see a small amount of larger pillars, less than that observed in Figure 5 for CPM and of smaller size (about the height of one clay layer), that expand the beidellite layers further apart than the average basal spacing of 16.5Å. Again, the layers are not rigid enough to maintain the larger basal spacing for any appreciable distance.

We know from using the CPM and CPH layers as molecular calipers of cation size that very large chromium polyoxocations were either present in the pillaring solution used to chromia pillar the higher charge density smectites beidellite and fluorohectorite, or that smaller chromium cations were further hydrolyzed (possibly by oxolation type reactions) in the lower charge density smectites. If the large chromium polyoxocations responsible for the CPM and CPH basal spacings were initially present in the pillaring solution, then they could have been hydrolytically degraded in the interlayer of the higher charge density smectites to achieve charge neutrality, since large chromium polyoxocations have a lower charge density than smaller chromium oxocations. The interlayer hydrolysis reaction would be the opposite of the reaction which generates the large polyoxocations, and is dependent upon the availability of protons. This reaction



could also be occurring in montmorillonite, and possibly hectorite, although to a much smaller extent. This follows from the results of Brindley and Yamanaka (22) and Carr (25), who both concluded that the montmorillonite layers hydrolyze intercalated chromium cations. We can extend this conclusion to other clay hosts of different layer charge, and see that as the magnitude of the layer charge increases, so does interlayer chromium hydrolysis, and the basal spacing of the final chromia pillared clay decreases.

One way to test the direction of the interlayer hydrolysis reaction is to compare the x-ray basal spacings resulting from a chromia pillared montmorillonite prepared by direct exchange of the pillaring solution (the usual procedure), with one prepared by in situ hydrolysis, i.e. where the smectite is present in the pillaring solution during aging. The xrd results of this experiment are shown in Figure 9, and it is clear that the in situ hydrolyzed CPM has a smaller gallery height and is less crystalline, or less ordered. This is most likely due to the clay layer charge increasing the proton concentration in the clay galleries, thus directing the chromium hydrolysis reaction to produce smaller cations. If the gallery environment were to promote hydrolysis in the forward direction, we would expect to see larger basal spacings for the in situ hydrolyzed CPM.

We believe this effect of increasing interlayer chromium hydrolysis with increasing layer charge density to



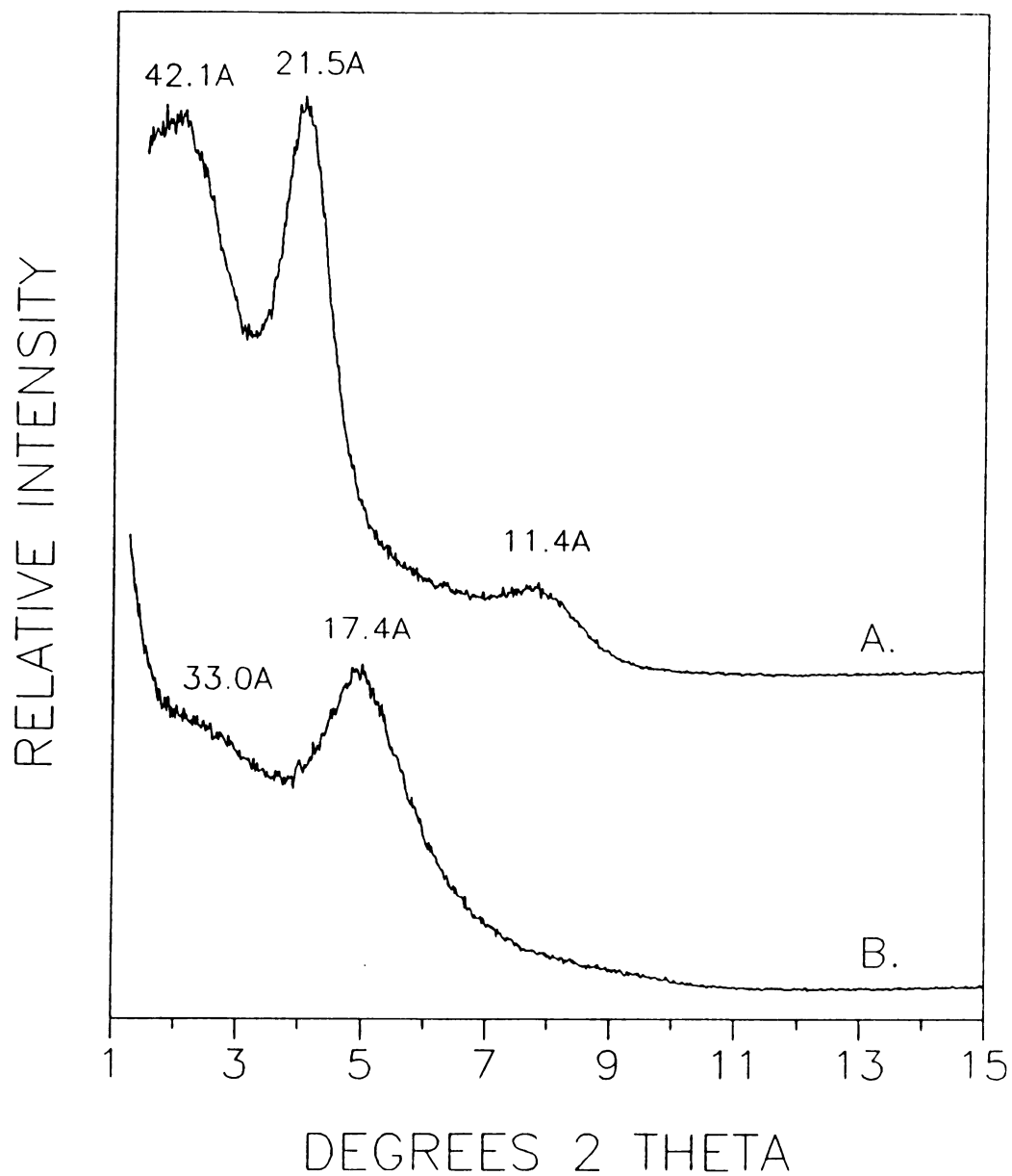


Figure 9. XRD patterns of CPM (350°C) prepared by:
A. Direct Exchange and B. In situ hydrolysis of
the chromia pillaring solution. Pillaring
solution aged at 100°C for 36 hours, OH/Cr=2.0.

outweigh the structural significance of the host clay being dioctahedral, such as montmorillonite and beidellite, or trioctahedral, such as hectorite and fluorohectorite. However, the availability and concentration of protons (Bronsted acidity) during interlayer hydrolysis should be greater for chromia pillared trioctahedral smectites, since protons could reside in the octahedral cavities of chromia pillared dioctahedral smectites. This proton availability should affect the equilibrium of chromium cation hydrolysis.

Layer charge proximity may also affect interlayer chromium oligomeric cation hydrolysis, since charge site location effects ion hydration (37). The source of layer charge in beidellite (125 meq/100g) resides in the tetrahedral sheet, which is closest to the gallery, and that for fluorohectorite (167 meq/100g) resides in the octahedral sheet, further from the gallery. The resulting CPB had only a 2.2\AA larger gallery height than CPF, even though the difference between the host clay cation exchange capacities is relatively large, 42 meq/100g. It is possible that the tetrahedrally charged beidellite exerts a stronger anionic force on the intercalated chromium oligomeric cations than would a charge of similar magnitude but of greater proximity to the gallery. This results in an effect similar to a higher charge density smectite.

To further confirm the effect layer charge has on chromia pillared smectite basal spacings, a series of reduced charge montmorillonites were prepared and chromia

pillared. The series consisted of 0% reduced charge montmorillonite (unaltered Na-montmorillonite), 10%, 20%, and 30% reduced charge Na,Li-montmorillonite. The x-ray diffraction patterns of the resulting reduced charge chromia pillared montmorillonites (RCCPM) are shown in Figure 10. There seems to be a limit of layer charge, somewhere between 80 and 66 meq/100g, where the smectite layers do not swell or exfoliate sufficiently for chromium polyoxocation exchange. This is likely due to the fact that reduced charge montmorillonite is heterogeneous with respect to layer charge distribution (38). However, at 10% charge reduction, or 80 meq/100g, the gallery height of RCCPM is indeed larger than that for non charge reduced CPM, and is similar to that for CPH. Therefore, two different clays of similar cation exchange capacities can be chromia pillared and result in a similar gallery height. At 30% charge reduction, 55 meq/100g, the smectite layers did not swell, and this was the only case where Na was detected during chemical analysis of a chromia pillared smectite.

A Ni^{+2} reduced charge montmorillonite has been pillared with alumina, yet the effect of the reduced charge was on the lateral spacing of the pillars, not on the basal spacings (39). However, the lateral spacing of reduced charge chromia pillared montmorillonite is most likely larger than that for non charge reduced chromia pillared montmorillonite.

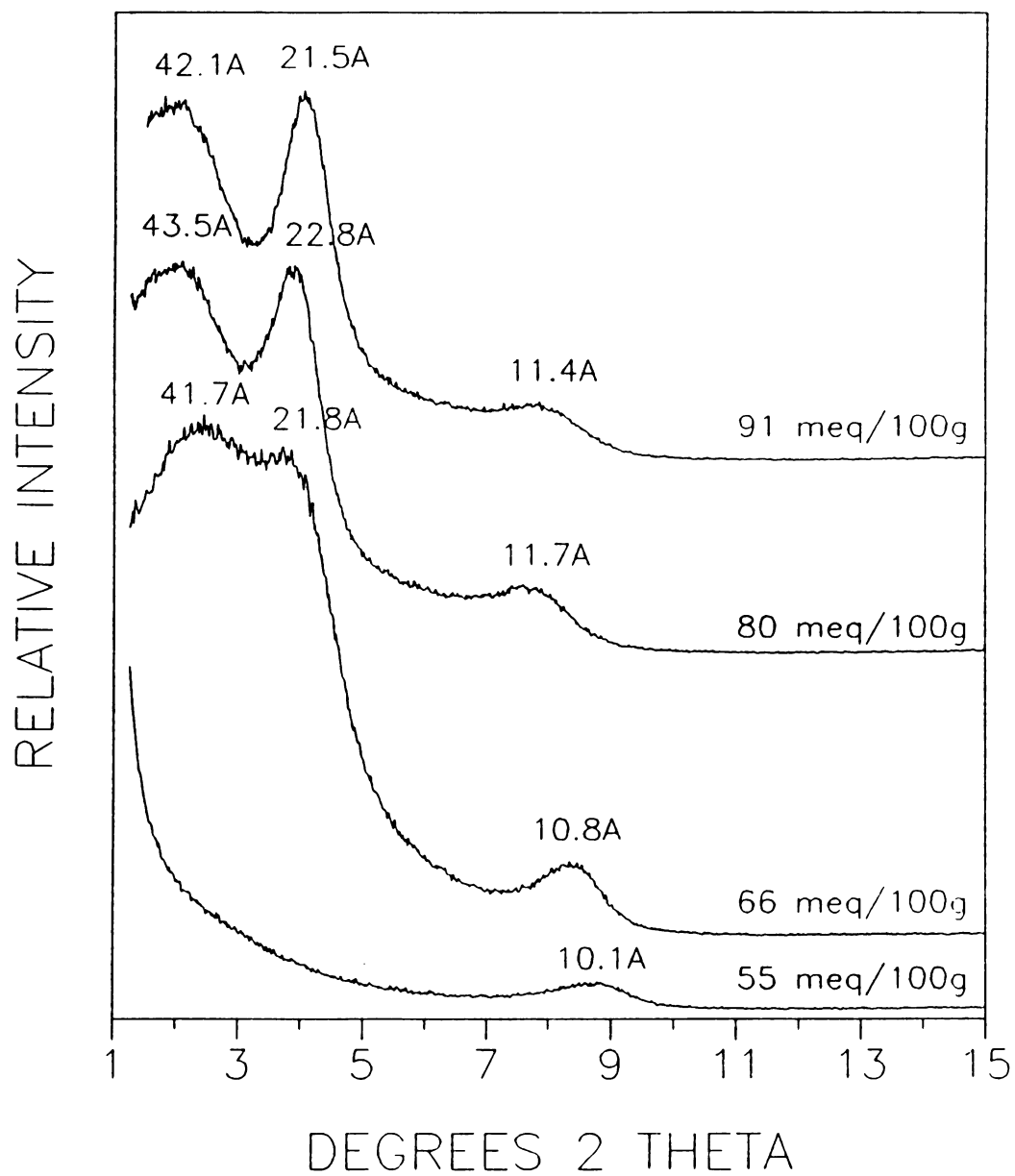


Figure 10. XRD patterns (350°) of 0-30% RCCPM. Pillaring solution aged at 100°C for 36 hours, $\text{OH/Cr}=2.0$.

A summary of the physical properties of the various chromia pillared smectites described herein is shown in Table 5. A similar decrease in x-ray basal spacings with increasing treatment temperature is observed for both direct exchanged CPM and CPH, however, CPB seems to maintain its small basal spacing somewhat better. This could be due to a stronger interaction of the pillars with the tetrahedrally charged clay layers of beidellite, a phenomenon observed previously for alumina pillared beidellite (40).

The increasing surface areas of both CPM and CPH with increasing outgassing temperature can be explained by thermal pillar migration in the galleries, thus causing an increase in both micropores and mesopores. Such an explanation coincides with the previously observed loss of layer order with increasing treatment temperature in the x-ray diffraction patterns. The surface areas of CPM, CPH, and CPB after only a 100°C outgassing are most likely artificially low due to the presence of interlayer water. However, after dehydration/dehydroxylation at 350 or 500°C, the surface areas correlate quite well with the basal spacings for all samples.

The surface areas of the higher charge density CPB are relatively constant with increasing outgassing temperature, due to minimal pillar migration. The surface areas at 350°C of the very high charge density CPF is smaller than that for CPB, which follows from CPF having the smallest x-ray basal spacing. Also, as the amount of charge reduction increased

Table 5. Physical properties of chromia pillared smectites (a).

Host	Temperature (°C)	d ₀₀₁ (Å)	Surface Area ^(b) (m ² /g)	Cr per unit cell
<u>Mont.</u>				
DE CPM ^(c)	100	53.8, 26.3	318	4.36
	350	42.1, 21.5	378	
	500	37.1, 20.1	573	
ISH CPM ^(d)	350	33.0, 17.4	322	3.52
10%RCCPM ^(e)	350	43.5, 22.8	368	
20%RCCPM	350	41.7, 21.8	351	
30%RCCPM	350	10.1	168	
<u>Hect.</u>				
CPH	100	50.0, 25.0	330	4.54
	350	44.0, 22.0	391	
	500	41.4, 20.7	588	
<u>Beid.</u>				
CPB	100	17.5	280	2.16
	350	16.5	254	
	500	16.3	245	
<u>Flhct.</u>				
CPF	350	14.3	177	

(a) Pillaring solution: OH/Cr=2.0, aged for 36 hours at 100°C.

(b) Samples were outgassed at the indicated temperature.

(c) Direct exchanged chromia pillared montmorillonite.

(d) In situ hydrolyzed chromia pillared montmorillonite.

(e) Reduced charge chromia pillared montmorillonite.



for the RCCPM samples, the resulting gallery heights and surface areas decreased.

CPH, with the largest x-ray basal spacing among the chromia pillared smectites studied, intercalated the most chromium, 4.54 Cr atoms per unit cell, while the slightly higher charge density CPM intercalated a similar amount, 4.36 Cr atoms per unit cell. If we were to assume that each pillared unit cell is surrounded by 6 unit cells without pillars, then there would be 7 unit cells per pillar. This would mean that each pillar is composed of roughly 30 Cr atoms. Since the CPM gallery height is roughly 12\AA , or 5 oxygen planes, and if there were 6-8 oxygen atoms per plane, then there would be 30-40 oxygen atoms per pillar. The pillars should have a Cr to oxygen ratio similar to that for Cr_2O_3 , therefore $(\text{Cr}_{26}\text{O}_{39}\text{H}_{4.6})^{4.6+}$ is likely, which is close to the plausible assumption that each pillar is composed of roughly 30 Cr atoms.

The in situ hydrolyzed CPM intercalated somewhat less chromium than direct exchanged CPM, 3.52 Cr atoms per unit cell versus 4.36, and had a smaller surface area. This may be due to the formation of smaller and higher charge density chromium polyoxocations in the montmorillonite galleries during the aging of the pillar precursor solution. The high charge density CPB only intercalated 2.16 Cr atoms per unit cell, which would be expected since CPB has a small basal spacing and surface area.

The large chromium polyoxocations, which constitute the pillar precursors, have been proposed by Spiccia and Stunzi to be made up of smaller Cr_3 or Cr_4 hydroxy complexes which act as basic building blocks (41-43). The actual composition of the Cr polyoxocation(s) responsible for the chromia pillared clay gallery heights (including the difficult to reproduce phase responsible for super gallery heights) is unknown, however, it is likely that they are the condensation products of trinuclear species, since the $\text{Cr}_3(\text{OH})_4(\text{H}_2\text{O})_9^{5+}$ cation was found to be more stable than either $\text{Cr}_2(\text{OH})_2(\text{H}_2\text{O})_8^{4+}$ or $\text{Cr}_4(\text{OH})_6(\text{H}_2\text{O})_{11}^{6+}$ (39). Figure 9 shows one possible structure for the Cr_3 cation.

Further experiments are now in progress to study the catalytic aromatization selectivity of these novel supported chromia catalysts.

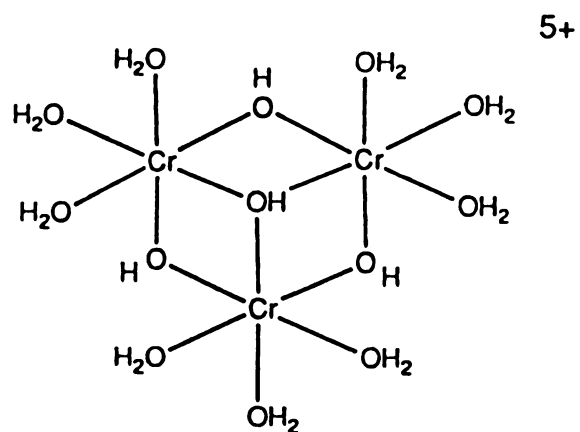
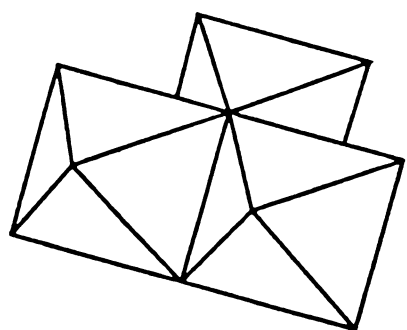


Figure 11. One possible structure of the trinuclear aqua chromium (III) cation, $\text{Cr}_3(\text{OH})_4(\text{H}_2\text{O})_9^{5+}$ (43).

REFERENCES

1. Moini, A. and Pinnavaia, T.J. Solid State Ionics **1988**, 26, 119.
2. Yamanaka, S.; Nishihara, T.; Hattori, M. Mater. Chem Phys. **1987**, 17, 87.
3. Pinnavaia, T.J. Science **1983**, 220, 365.
4. Pinnavaia, T.J. in Chemical Reactions in Organic and Inorganic Constrained Systems, **1986**, R. Setton, ed., Reidel, 151-164.
5. Figueras, F. Catal. Rev. Sci. Eng. **1988**, 30, 457.
6. Brindley, G.W. and Sempels, R.E. Clay Miner. **1977**, 12, 229.
7. Vaughan, D.E.W. and Lussier, R.J. in Proceedings 5th International Conference on Zeolites, Naples, Italy, **1980**, L.V.C. Rees, ed., Heyden, London, 94-101.
8. Hopkins, P.D.; Meyers, B.L.; Van Duch, D.M. U.S. Patent 4,452,910, **1984**.
9. Yamanaka, S. and Brindley, G.W. Clays Clay Miner. **1979**, 27, 119.
10. Burch, R. and Warburton, C.I. J. Catal. **1986**, 97, 503.
11. Sterte, J. Clays Clay Miner. **1986**, 34, 658.
12. Lewis, R.M.; Ott, K.C.; Van Santen, R.A. U.S. Patent 4,510,257, **1985**.
13. Lahav, N.; Shani, U.; Shabtai, J. Clays Clay Miner., **1978**, 26, 107.
14. Pesquera, C.; Gonzalez, F.; Benito, I.; Mendioroz, S.; Pajares, J.A. Appl. Catal., **1991**, 69, 97.
15. Barrer, R.M. J. Inclus. Phen., **1986**, 4, 109.
16. Carrado, K.A.; Suib, S.L.; Skoularikis, N.D.; Coughlin, R.W. Inorg. Chem. **1986**, 25, 4217.
17. Skoularikis, N.D.; Coughlin, R.W.; Kostapapas, A.; Carrado, K.; Suib, S.L. Appl. Catal. **1988**, 39, 61.

18. Lussier, R.J.; Magee, J.S.; Vaughan, D.E.W. in Preprints 7th Canadian Symposium on Catalysis, Edmonton, 1980, S.E. Wauke and S.K. Chakrabartty, eds., Alberta Research Council, Edmonton, Alberta, 88-95.
19. Occelli, M.L. Ind. Eng. Chem. Prod. Res. Dev. 1983, 22, 553.
20. Shabtai, J.; Lazar, R.; Oblad, A.G. in Proceedings of the 7th International Congress on Catalysis, 1981, T. Seiyama and K. Tanabe, eds., Kodansha-Elsevier, Tokyo, 828-840.
21. Occelli, M.L. in Proceedings of the International Clay Conference, Denver, 1987, L.G. Schultz, H. van Olphen, and F.A. Mumpton, eds., The Clay Minerals Society, Bloomington, Indiana, 319-323.
22. Brindley, G.W. and Yamanaka, S. Amer. Miner. 1979, 64, 830.
23. Rengasamy P. and Oades, J.M. Aust. J. Soil Res. 1978, 16, 53.
24. Baes, C.F. and Mesmer, R.E. The Hydrolysis of Cations, 1976, Wiley, New York, 211-219.
25. Carr, R.M. Clays Clay Miner. 1985, 33, 357.
26. Koppelman, M.H. and Dillard, J.G. Clays Clay Miner. 1980, 28, 211.
27. Pinnavaia, T.J.; Tzou, M.S.; Landau, S.D. J. Am. Chem. Soc. 1985, 107, 4783.
28. Tzou, M.S. and Pinnavaia, T.J. Catal. Today 1988, 2, 243.
29. Brindley, G.W. and Ertem, G. Clays Clay Miner. 1971, 19, 399.
30. Busenberg, E. and Clemency, C.V. Clays Clay Miner. 1973, 21, 213.
31. Springborg, J. Advances in Inorganic Chemistry, A.G. Sykes, ed., 1988, 32, Academic Press.
32. Kim, H.; Jin, W.; Lee, S.; Zhou, P.; Pinnavaia, T.J.; Mahanti, S.D.; Solin, S.A. Phys. Rev. Lett. 1988, 60, 2168.
33. Singh, S.S.; Kodama, H. Clays Clay Miner. 1988, 36, 397.

34. Occelli, M.L. and Lynch, J. J. Catal. **1987**, 107, 557.
35. Shabtai, J.; Rosell, M.; Tokarz, M. Clays Clay Miner. **1984**, 32, 99.
36. Brody, J.F.; Johnson, J.W.; McVicker, G.B.; Ziemiak, J.J. Solid State Ionics **1989**, 32/33, 350.
37. Mortland, M.M. and Raman, K.V. Clays Clay Miner. **1968**, 16, 393.
38. Clementz, D.M.; Mortland, M.M.; Pinnavaia, T.J. Clays Clay Miner. **1974**, 22, 49.
39. Suzuki, K.; Horio, M.; Mori, T. Mat. Res. Bull. **1988**, 23, 1711.
40. Plee, D.; Gatineau, L.; Fripiat, J.J. Clays Clay Miner. **1987**, 35, 81.
41. Stunzi, H. and Marty, W. Inorg. Chem. **1983**, 22, 2145.
42. Spiccia, L.; Marty, W.; Giovanoli, R. Inorg. Chem. **1988**, 27, 2660.
43. Stunzi, H.; Spiccia, L.; Rotzinger, F.P.; Marty, W. Inorg. Chem. **1989**, 28, 66.



CHAPTER III
CATALYTIC PROPERTIES OF
CHROMIA PILLARED CLAYS

INTRODUCTION

Weisz and Frilette (1) first reported molecular shape selective zeolite catalysis in 1960. Since then most reports concerning shape selectivity have focused mainly on the industrially important zeolite catalysts (2-4). It is now recognized that molecular shape selectivity can arise from a number of factors; including, diffusional effects, steric constraints, and coulombic field interactions. The unique nanoporous environment afforded by metal oxide pillared clays should impose a steric and/or electronic effect on the catalyzed reaction. Simple cation exchanged montmorillonites, which have been studied as heterogeneous catalysts for some organic reactions(5), are typically non-nanoporous.

Various metal oxide pillared clays are now known to be effective cracking catalysts (6,7). The current goal is to develop an inorganic polycation pillared material with a pore opening larger than zeolite Y. Such materials can crack heavy gas oil fractions and are also able to withstand harsh thermal and hydrothermal regeneration conditions.

Recently, an aluminum pillared rectorite showed both thermal and hydrothermal stabilities that surpassed aluminum pillared smectites, and even zeolite cracking catalysts (8). Delaminated clay cracking catalysts with macroporosity have also been prepared (9), and now composite pillared clays are being synthesized (10,11). For example, tricomposite Al-Zr-B pillared clay showed higher catalytic cracking activity for a gas oil than either aluminum pillared clay or the bicomposites Al-Zr and Al-B pillared clay. A comparison of the acid catalytic properties of aluminum pillared montmorillonite and beidellite showed the latter to be more active due to the presence of Bronsted acidity arising from proton attack of the Si-O-Al linkages in the tetrahedral sheet (12). Vaughan (13) has recently reviewed the use of new pillar and sheet compositions in order to prepare pillared clays with desirable catalytic properties.

Much of the catalytic research interest of pillared clays has focused on catalytic cracking reactions, yet the potential exists for certain pillared clays to be shape selective catalysts. For example, Al, Zr, and Cr pillared montmorillonite catalyze molecular rearrangement reactions of glycols and oximes (14). Suzuki and Mori (15) have altered the lateral spacing of the pillars in alumina pillared montmorillonite by reducing the cation exchange capacity through calcination of a Na,Ni-montmorillonite. The resulting alumina pillared montmorillonite, with a larger lateral separation of the pillars, was used to



alkylate toluene with methanol. The reduced charge clay showed a slower rate of deactivation (16). This material also exhibited a restricted transition state type of shape selectivity for the disproportionation of m-xylene (17).

Supported chromium catalysts are best known for their industrial importance in the polymerization of ethylene (Phillips process). However, chromia is also known to be a versatile acid, hydrogenation, dehydrogenation, or aromatization catalyst (18). Recently, chromia pillared montmorillonite has been shown to be a selective oxidation catalyst for alcohols (19).

In the present study, we have investigated the selectivity of chromia pillared clays for the aromatization of n-octane to xylene isomers. Our objective was to utilize the effect of the unique pore environment of chromia pillared clays (20) on the distribution of isomers, particularly the industrially important p-xylene. We also have included a study of the selectivity of chromia pillared clays for n-decane cracking as well as gas oil cracking. The interesting product distributions we obtained can be explained by the ability of chromia pillared clays to act as solid acid catalysts and by the effect of the gallery environment on the electronic state of the reactants.

EXPERIMENTAL

Materials

Wyoming montmorillonite (SWy-1) was obtained from Source Clay Minerals Repository at the University of Missouri, Columbia, Mo. Montmorillonite was further purified by preparing a two weight percent aqueous suspension, which sedimented overnight to obtain the size fraction consisting of less than or equal to 2 micron particles. The clay fraction was then sodium exchanged by mixing with a 20-fold excess of NaCl at room temperature for one hour. The clay was then dialyzed until a negative silver nitrate test was obtained for chloride ion. Chemical analysis of the resulting purified Na-montmorillonite indicated a unit cell formula of $\text{Na}_{0.66}[\text{Al}_{3.12}\text{Fe}_{0.40}\text{Mg}_{0.48}](\text{Si}_{7.82}\text{Al}_{0.18})\text{O}_{20}(\text{OH})_4$.

Na-beidellite, of structural formula $\text{Na}_{0.90}[\text{Al}_{4.00}](\text{Si}_{7.10}\text{Al}_{0.90})\text{O}_{20}(\text{OH})_4$, was provided by George Poncelet from the Université Catholique de Louvain.

Ca-hectorite was obtained by the Source Clay Minerals Repository (SHCa-1), and was further purified and sodium exchanged using the same procedure as that for montmorillonite. The unit cell formula for purified Na-hectorite was $\text{Na}_{0.62}[\text{Mg}_{5.38}\text{Li}_{0.62}](\text{Si}_{8.00})\text{O}_{20}(\text{OH})_4$.

The synthetic Li-fluorohectorite used in this work had a unit cell formula of $\text{Li}_{1.24}[\text{Mg}_{4.76}\text{Li}_{1.24}](\text{Si}_{8.00})\text{O}_{20}(\text{OH})_4$.

A commercial chromia supported on alumina catalyst was obtained from Chemical Dynamics Corporation. The chromia loading was 19 wt. % and the surface area was $7.7 \text{ m}^2/\text{g}$.

Pillaring Reactions

The synthesis of the chromia pillared smectites used in this study were similar to those described previously (20). In order to pillar one gram of purified Na-montmorillonite, 200 ml of a 0.25M aqueous Na_2CO_3 solution was added dropwise to 300 ml of a 0.17M aqueous $\text{Cr}(\text{NO}_3)_3$ solution (60 moles of chromium per clay exchange equivalent), until the final Cr concentration was 0.10M and the OH/Cr ratio was 2.0. The pillaring solution was allowed to age for 36 hours at either room temperature or 100°C , after which a 1 wt % aqueous purified Na-montmorillonite suspension was added. The chromium polyoxocations were allowed to exchange for the sodium cations in the montmorillonite interlayers by stirring the resulting mixture for 1.5 hours. The pillaring solution formed by aging at room temperature afforded a chromium exchanged clay with a basal spacing of 12.3\AA (Designated RTH-CPM). However, the pillaring solution aged at 100°C gave a pillared product with a basal spacing of 21.5\AA (Designated DE-CPM). In an alternative synthesis procedure, the pillaring solution was aged at 100°C in the presence of the aqueous clay suspension, i.e. in-situ hydrolysis (ISH-CPM), resulting in a 17.4\AA product. Each chromium exchanged clay was washed free of excess salt by



repeated centrifugation/dispersion cycles until flocculated particles were present, and then air dried on a glass sheet. The resulting film was dehydrated/dehydroxylated at 350°C under inert gas (nitrogen or argon), ground in a mortar and pestle, and sieved to a particle size of 250-500 microns.

A series of reduced charge montmorillonite samples were prepared by the method of Brindley and Ertem (21). One wt % aqueous suspensions of Na- and Li- montmorillonite were mixed in the following proportions to achieve the desired levels of charge reduction: 100:0, 90:10, 80:20, 70:30. The suspensions were stirred for 24 hours to allow randomization of the ions and then air dried on glass sheets. The resulting films were heated for 24 hours at 220°C in an oven to achieve layer charge reduction by migration of Li^+ cations to empty octahedral sites in the layer. The reduced charge montmorillonite samples were then suspended in water at 1 wt % and dispersed in a blender.

Aqueous suspensions (1.0 wt %) of Na-beidellite, Na-hectorite, Li-fluorohectorite, and Na,Li-reduced charge montmorillonite were chromium exchanged and pillared following the procedure given for direct exchanged chromia pillared montmorillonite (DE-CPM). In each case the amount of $\text{Cr}(\text{NO}_3)_3$ used per gram of smectite was adjusted such that the moles of chromium per clay exchange equivalent was 60. The resulting chromia pillared beidellite, chromia pillared hectorite, chromia pillared fluorohectorite, and reduced

charge chromia pillared montmorillonite are referred to as CPB, CPH, CPF and RCCPM respectively.

Alumina pillared montmorillonite (APM) was synthesized according to a previously published procedure (22). The pillaring solution was an aqueous dilution of Chlorhydrol, or aluminum chlorohydrate, which was obtained from Reheis Chemical Co. The final concentration of the pillaring solution was 0.23M, which corresponded to a OH/Al ratio of 2.50. The Al pillaring solution was stirred with purified Na-montmorillonite such that the mmoles Al^{3+} /meq clay was 4.6, then washed, dried, and calcined.

Physical Methods

X-ray diffraction patterns were obtained using a Rigaku rotating anode x-ray diffractometer equipped with CuK alpha radiation. Oriented thin film samples were prepared for x-ray analysis by air drying on a glass slide approximately 1 ml of a 1 wt.% freshly prepared pillared clay aqueous suspension. The slides were heated to the desired temperature (100, 350, or 500°C) under inert gas for 2 hours.

Nitrogen adsorption/desorption isotherms were obtained at -196°C with either a Quantachrome Autosorb or a Quantasorb Jr. sorption analyzer using ultra high purity N_2 gas as the adsorbate and He as the reference or carrier. Approximately 100 mg samples were outgassed at 350°C under vacuum for 12 hours prior to analysis.

Total acidity was measured through pyridine adsorption on pelletized chromia pillared clay samples in a McBain microbalance. Samples were loaded into glass buckets suspended on quartz springs (spring constant = 1cm/50mg), outgassed at 350°C and 1×10^{-4} torr for 10 hours, then allowed to cool to room temperature. Degassed pyridine was then allowed to adsorb onto the samples at an equilibrium vapor pressure at room temperature. The samples were evacuated to remove physisorbed pyridine, and then heated incrementally to 350°C, while measuring the change in the spring length.

Bronsted and Lewis acidity were analyzed by FTIR using an enclosed sample cell equipped with both pyridine and vacuum outlets. An oriented thin film of pillared clay was mounted on a silicon disk window, outgassed at 350°C for 2 hours, and then allowed to cool to room temperature. Pyridine was then allowed to interact with the sample at room temperature using a similar procedure to that described for the adsorption experiments. The cell was evacuated to remove physisorbed pyridine, then the cell temperature was increased in 25°C intervals. FTIR spectra were obtained at each temperature interval.

Elemental analysis of the host smectites were performed on a Jarrell-Ash 955 Atom-Comp ICP-AES. Clay samples (0.05 g) were prepared for analysis by fusion with lithium borate (0.3 g, Aldrich, Gold Label) in graphite crucibles at 1000°C for 12 minutes. The resultant glass was transferred to 100

ml of 5% HNO_3 and mixed until completely dissolved. NIST plastic clay 98a served as a standard. Galbraith Laboratories, Inc. analyzed chromium pillared clay samples for Si, Al, Mg, and Cr. The amount of intercalated Cr per $\text{O}_{20}(\text{OH})_4$ unit was calculated based on the assumption that the Si content of the host clay remained constant throughout the pillaring reaction. Galbraith Laboratories, Inc. also analyzed spent catalyst samples for hydrogen and carbon.

Catalytic Methods

Decane cracking and octane aromatization catalytic studies were performed with a continuous flow microreactor, as shown in Figure 12. All delivery lines were composed of 316 stainless steel tubing. Gold label grade n-octane and n-decane were obtained from Aldrich and were used without further purification. The reactant liquid was delivered to the top of a vertically mounted tube furnace via a syringe pump. The reactant weight hourly space velocity (g reactant/hr/g Cr_2O_3) was 2.5 hour^{-1} . High purity helium was used as the carrier gas. The helium was further purified by flowing through molecular sieves and a color-indicating oxygen trap. The contact time (volume catalyst bed/carrier gas flow rate) was 1.5 seconds. Either high purity CO or H_2 was substituted for He for pre-reduction of the catalyst. The prereduction contact time was 1.5 seconds and the reduction interval was 2 hours. All reactions were carried out at atmospheric pressure and at 500°C , unless otherwise

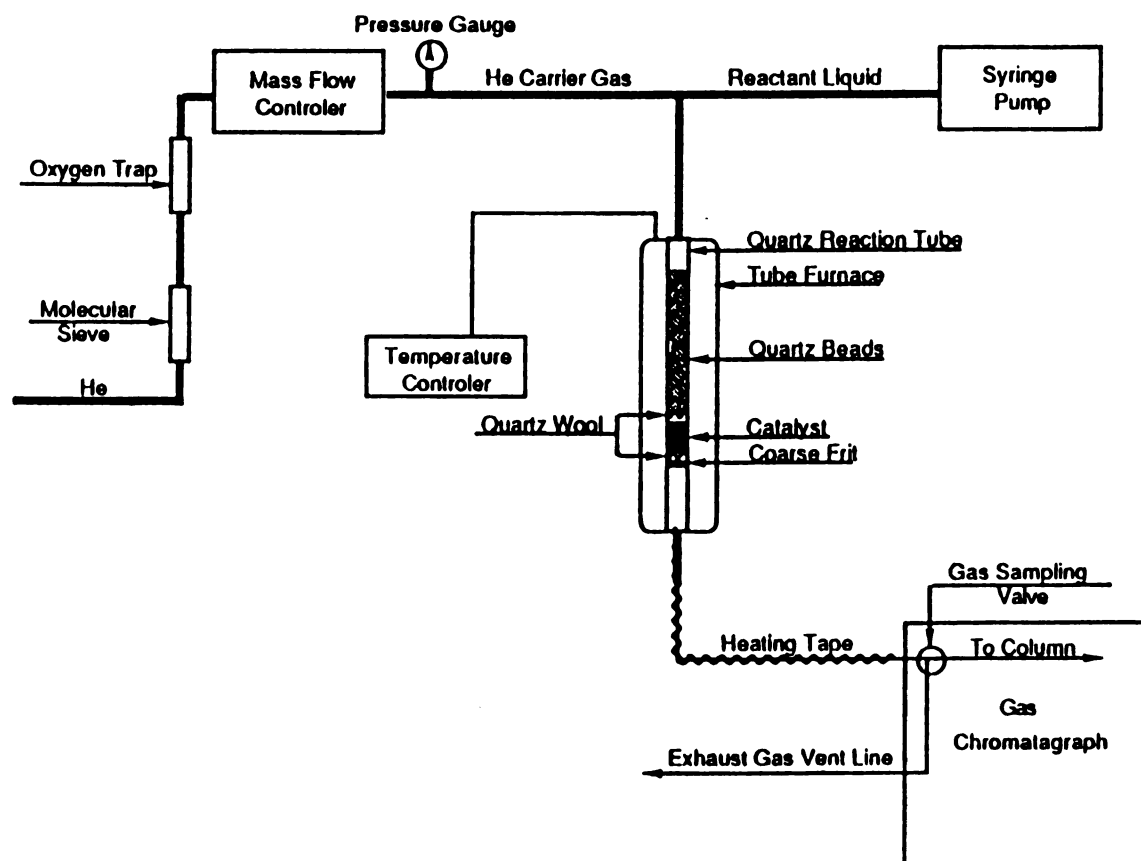


Figure 12. Schematic diagram of the continuous flow microreactor used for catalyst testing.

noted. The reaction products were kept in the gaseous state with the use of an electrically heated transfer line, and were injected by a gas sampling valve into an HP 5890 gas chromatograph. The column used was a Supelcowax 10 glass capillary column, 30 meters long X 0.75 millimeters inside diameter. The gas chromatograph oven temperature was 60°C, and the injector and thermal conductivity detector temperatures were 250°C.

A microactivity test reactor was prepared according to ASTM Designation: D 3907-87, to compare the fluid catalytic cracking activity of various pillared clay catalysts. The gas oil charge stock with a density of 0.93 g/ml was donated by Amoco Oil Company. The only deviation from the ASTM standard was the use of 0.6 g of catalyst material instead of the recommended use of 4 g. However, the catalyst to feed mass ratio of 3 was not altered. Product analysis was obtained by gas chromatography using a simulated distillation technique described by Test Method D 2887. The measured conversion was calculated using the equation:

$$\text{Weight \% conversion} = \frac{F - (R \times L)/100 - H}{F} \times 100$$

where:

F = gas oil feed in g,

R = weight percentage of material boiling above 216°C in liquid product receiver,

L = g of liquid product in receiver,

H = liquid holdup in g at exit line and receiver joint.

RESULTS

Acidity

The reaction of Na^+ -montmorillonite with a hydrolyzed Cr^{3+} solution ($\text{OH}^-/\text{Cr} = 2.0$) aged 36 hours at 100°C afforded a large gallery chromia pillared clay. The basal spacing of the product, designated DE-CPM, after calcination at 350°C was 21.5\AA and the BET surface area was $378\text{ m}^2/\text{g}$. The acidity of DE-CPM was examined by pyridine chemisorption. Figure 13 shows that the amount of bound pyridine decreases more or less linearly with increasing temperature. However, approximately 10^{19} acid sites for pyridine chemisorption remain per gram of DE CPM at 350°C .

On the basis of infrared stretching vibrations using the band assignments of Ward (23) for protonated and coordinated pyridine (see Figure 14), the acidity is mainly of the Lewis type, though some Bronsted acidity is also present. The assignments are: physisorbed pyridine (1434 and 1485 cm^{-1}), hydrogen-bonded pyridine (1590 cm^{-1}), Lewis-bound pyridine (1445 , 1485 , 1578 , 1590 and 1613 cm^{-1}), and the pyridinium cation (1485 , 1540 , 1606 , and 1635 cm^{-1}). The Bronsted acidity is the first to diminish with increasing temperature.

Related materials were synthesized similar to DE-CPM, except that the Cr^{3+} pillaring solution was aged at room temperature instead of 100°C . The product, designated RTH-CPM, had a basal spacing of 12.3\AA after calcination at 350°C .

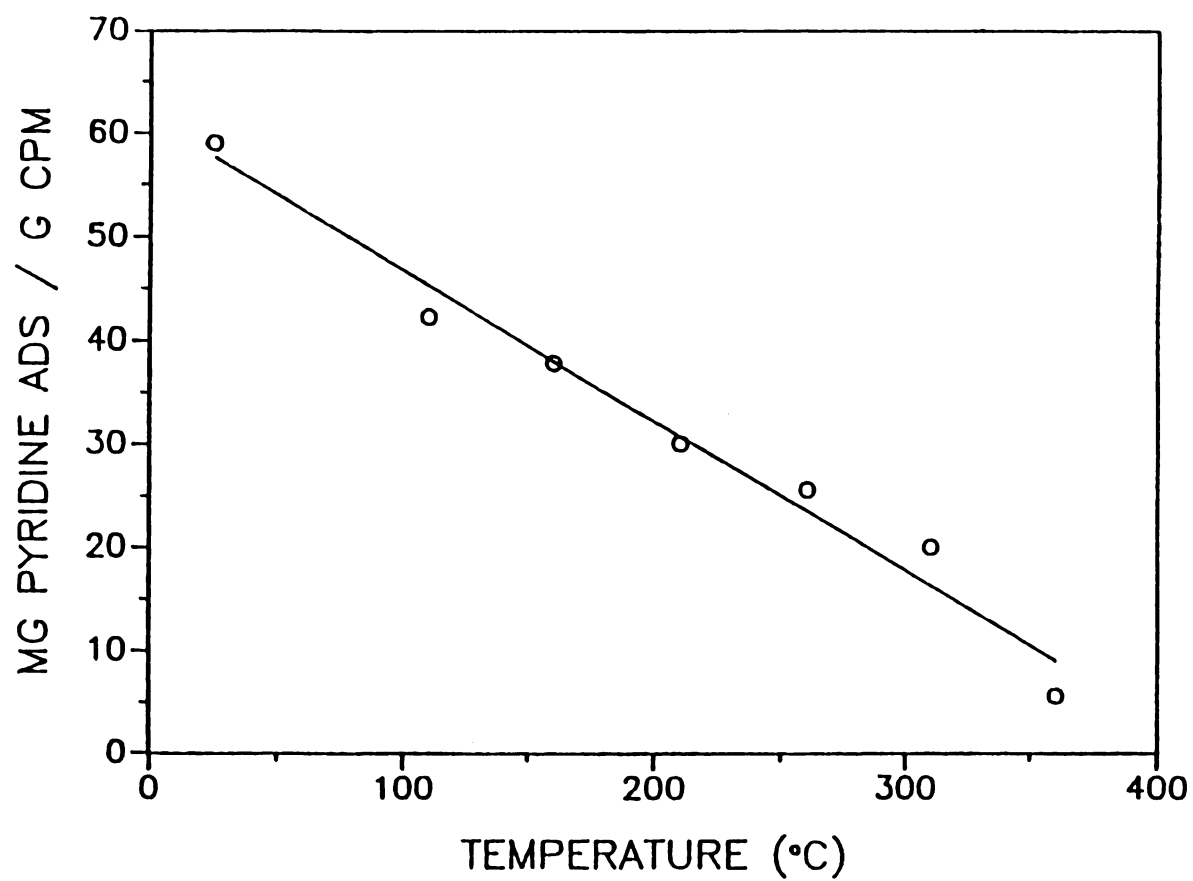


Figure 13. Temperature dependent acidity of chromia pillared clay (DE-CPM) as measured by pyrdine adsorption.

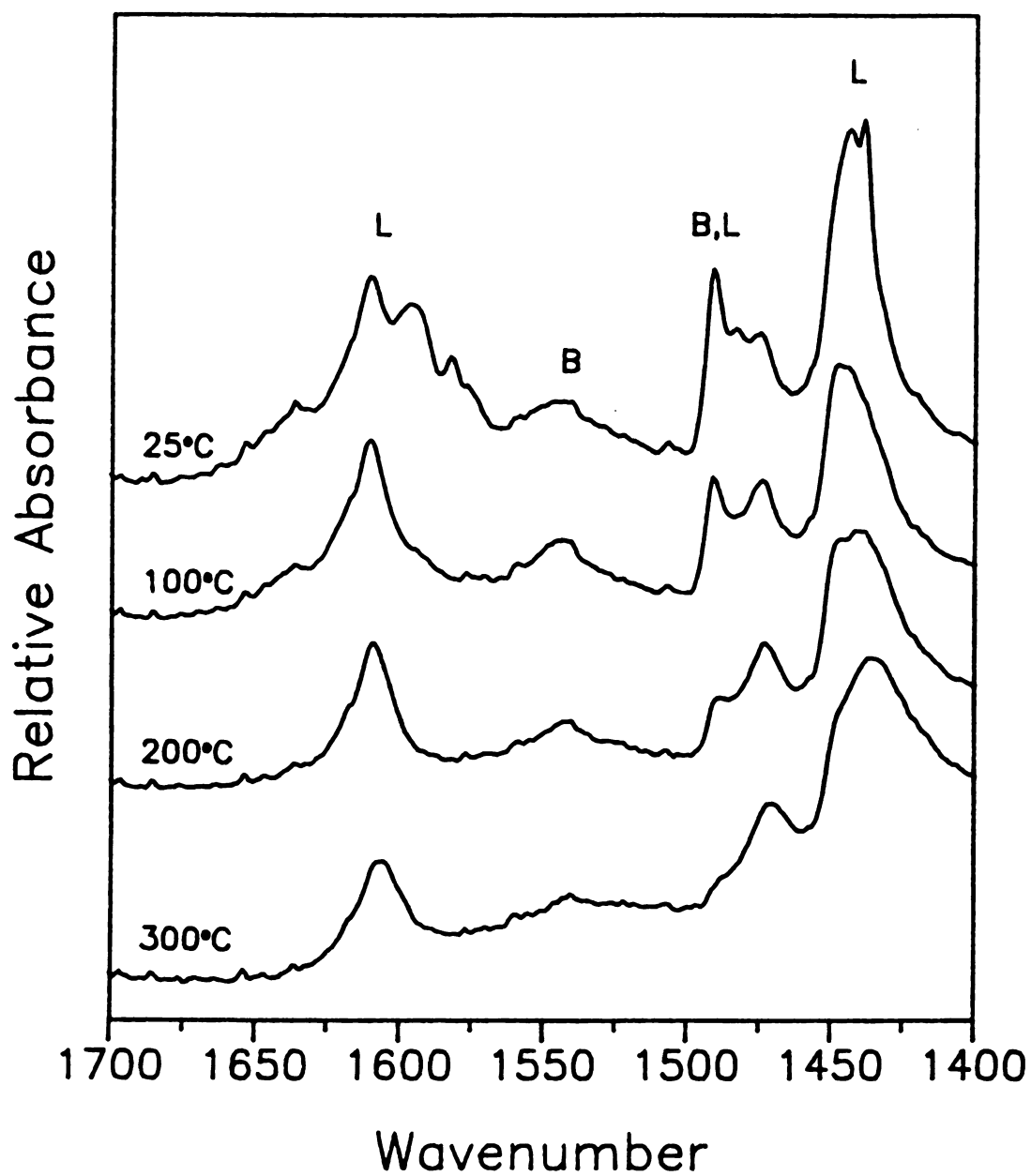


Figure 14. Temperature dependent FTIR spectra of pyridine adsorbed on DE-CPM. L: Lewis bound pyridine, B: Bronsted bound pyridine. Spectra were recorded at the temperature shown.

and a BET surface area of $110 \text{ m}^2/\text{g}$. The RTH-CPM showed a negligible amount of pyridine chemisorption.

Cracking Reactions

Two reactions, microactivity test (MAT) cracking of a gas oil and decane cracking, were used to probe catalytic acidity.

As shown in Table 6, chromia pillared montmorillonite (DE-CPM) exhibits MAT conversion properties similar to those for alumina pillared montmorillonite (APM). The APM does show slightly greater gasoline selectivity, which might be expected due to the strong acidity of the alumina pillars (24). The spent DE-CPM exhibited an exceptionally large carbon to hydrogen ratio, indicative of extensive coking. When the catalyst was regenerated at 600°C in air to oxidize the coke, the mass of the spent catalyst was reduced by 10 percent, the basal spacing of the catalyst decreased from 21.5\AA to 16.8\AA , and the BET surface area increased from $378 \text{ m}^2/\text{g}$ to $580 \text{ m}^2/\text{g}$. It should be noted that a BET surface area increase accompanying large treatment temperatures has been seen previously (20) and is most likely due to an increase in non-microporous surface area arising from pillar migration. The regenerated CPM (REG-CPM) showed the same conversion as fresh catalyst, but had little or no gasoline selectivity in the carbon number range of 5-10. Most of the converted products had a carbon chain length greater than 10, and they mainly accumulated in the reactor exit line.

Table 6. MAT results for gas oil cracking over chromia pillared montmorillonite and alumina pillared montmorillonite (APM).

Catalyst	Basal Spacing (Å)	Surface Area (m ² /g)	Measured Conv. Weight %	Liquid Product Gasoline Select.	Spent Catalyst Wt% C	Spent Catalyst Wt% H
DE-CPM	21.5	378	59	82	8.13	0.99
REG-CPM(a)	16.8	580	59	0		
RTH-CPM	12.3	110	50	0	0.59	0.77
APM	19.2	322	58	87		

(a) Regenerated chromia pillared montmorillonite: DE-CPM catalyst regenerated by heating to 600°C (10 °C/min) for 2 hours.

The 12.3Å phase of the smaller gallery height room temperature hydrolyzed chromia pillared montmorillonite (RTH-CPM) showed the lowest MAT conversion of the catalysts tested, and no gasoline selectivity. Very little fouling, or coking, was evidenced by the low carbon to hydrogen ratio for the used catalyst. Again, as was the case for the REG-CPM, most of the converted products were long chain hydrocarbons which became trapped in the reactor exit line.

Table 7 shows the product distributions for the catalytic cracking of n-decane over two chromia pillared clays, DE-CPM and CPH. Included for comparison are the results for a commercial chromia on alumina catalyst. At 500°C the DE-CPM catalyst showed much higher activity than the commercial Cr/Alumina catalyst. The main reaction product for the DE-CPM catalyst was C₂ hydrocarbons, whereas the Cr/Alumina catalyst gave substantially greater yields of C₁₀ isomers (other than n-decane) and C₉ products. The DE-CPM also produced alkylated products >C₁₀ which were not measured as coke. At 350°C the Cr/Alumina catalyst showed virtually no activity, while DE CPM showed moderate conversion and an improved selectivity in the C₃-C₆ range, as compared to the selectivity at 500°C. The chromia pillared hectorite (CPH), with a basal spacing of 22.0Å at 350°C, showed the highest activity. This latter catalyst was also selective toward cracked products in the C₃-C₆ range, with virtually no alkylated products >C₁₀.

Table 7. Decane cracking product distributions of CPM, CPH, and a commercial chromia on alumina catalyst^(a).

	<u>DE CPM</u>	<u>Cr/Alumina</u>	<u>DE CPM</u>	<u>Cr/Alumina</u>	<u>CPH</u>
Temp (°C)	500	500	350	350	350
d ₀₀₁ (Å)	20.1	-	21.5	-	22.0
BET (m ² /g)	573	7.7 ^(b)	378	7.7 ^(b)	391
Conversion ^(c)	57.4	9.5	21.0	<1	73.4
C ₂	43.6	18.4	1.8	-	1.4
C ₃	10.9	7.2	11.2	-	12.4
C ₄	4.5	4.2	25.8	-	29.8
C ₅	4.6	4.3	21.6	-	31.7
C ₆	7.7	12.8	34.3	-	21.9
C ₇	4.2	5.3	0.8	-	0.8
C ₈	4.6	5.0	1.1	-	1.2
C ₉	3.5	17.5	2.8	-	0.7
C ₁₀	4.6	25.3	0.2	-	0.1
>C ₁₀	11.7	-	0.3	-	0.1

(a) n-decane weight hourly space velocity=2.5 hour⁻¹, He carrier gas contact time=1.5 sec, no prereduction. All values are in mole percent after 5 min time on stream.

(b) This surface area value was supplied by the manufacturer.

(c) Total conversion of n-decane.

Octane Aromatization

The ability of the chromia pillars to catalyze the aromatization of paraffins by dehydrocyclization was probed by studying n-octane aromatization.

Table 8 summarizes the catalytic results for n-octane aromatization over various chromia pillared montmorillonites, a chromia pillared hectorite, and a commercial chromia on alumina catalyst. Similar conversion was observed for all catalysts, except RTH-CPM with a small gallery height ($d_{001}=12.3\text{\AA}$) and the non-pillared 30% RCCPM, both of which showed low activity. The most active catalyst was a large gallery (22.8\AA basal spacing) chromia pillared montmorillonite which resulted from pillaring a clay host with a reduced cation exchange capacity (80 meq/100g).

Comparing the aromatic selectivity of converted products for the catalysts at similar conversion levels, the commercial chromia on alumina catalyst exhibited 16% higher aromatization selectivity than that of the most selective chromia pillared clay, 10% RCCPM. The chromia pillared montmorillonite resulting from in-situ hydrolysis of the pillaring solution (ISH-CPM) showed the lowest aromatization selectivity. All of the chromia pillared clays showed a much greater selectivity towards meta- and para-xylene than the chromia on alumina catalyst. However, the chromia on alumina catalyst was most selective towards ethyl benzene and ortho-xylene. In addition, the lower charge and larger

Table 8. Aromatization of n-octane over CPM, CPH, and a commercial chromia on alumina catalyst(a).

Catalyst	d ₀₀₁ (Å)	BET (m ² /g)	Conv(b)	Arom Select.	--Composition of Arom. Fraction(c) -- [Benz. Tol. E.B. o- m- p-Xyl]		
DE CPM	21.5	378	20	33	6.7	11.5	9.7 27.1 29.3 15.8
ISH CPM	17.4	322	26	27	6.4	15.3	8.0 25.2 30.6 14.5
RTH CPM	12.3	110	<1	0	0	0	0 0 0
10% RCCPM	22.8	368	19	37	7.1	11.0	11.9 31.5 25.4 13.1 3
20% RCCPM	21.8	351	28	36	8.2	12.8	11.6 31.1 23.7 12.7
30% RCCPM	10.1	168	9	27	9.7	10.6	16.8 37.4 16.6 8.9
CPH	22.0	391	22	33	8.7	9.1	15.2 34.8 21.4 10.8
Cr/Alumina	-	7.7	21	53	10.1	9.5	31.3 45.8 1.5 1.8

(a) All values are in mole percent after 5 min time on stream.

(b) Total conversion of n-octane to all products: cracked, isomerized, and aromatized.

(c) Composition of aromatic fraction: benzene, toluene, ethyl benzene, o-xylene, m-xylene, p-xylene.

pore chromia pillared clays: 10% RCCPM, 20% RCCPM, and CPH, show a greater selectivity towards ethyl benzene and ortho-xylene than either DE-CPM and ISH-CPM. Benzene and toluene selectivities, which are both products due to a combination of cracking and aromatization, were fairly constant, with ISH-CPM showing the highest selectivity for toluene and the lowest selectivity for benzene.

Figure 15 depicts the slightly decreasing aromatization selectivity over time for a DE-CPM catalyst regardless of prereduction. Carbon monoxide prereduction of the chromia pillars results in higher aromatization selectivity than hydrogen prereduction, and as the equations show in Figure 15, carbon monoxide is the only reductant which does not produce water as a product. The last equation in Figure 15 shows that hydrocarbons, such as n-octane, can be considered as a reductant to the chromia pillars.

Table 9 summarizes the effects of prereducing various chromia catalysts on n-octane aromatization. For DE-CPM, catalyst prereduction increases both conversion and aromatic selectivity, with carbon monoxide being more effective than hydrogen. However, as aromatization selectivity increases, so does the ethyl benzene and o-xylene make-up of the aromatic fraction, with a corresponding decrease in the meta- and para-xylene selectivity.

The carbon monoxide prereduced DE-CPM catalyst was regenerated after 30 minutes time on stream by heating the catalyst to 600°C in air for 2 hours, which oxidized and

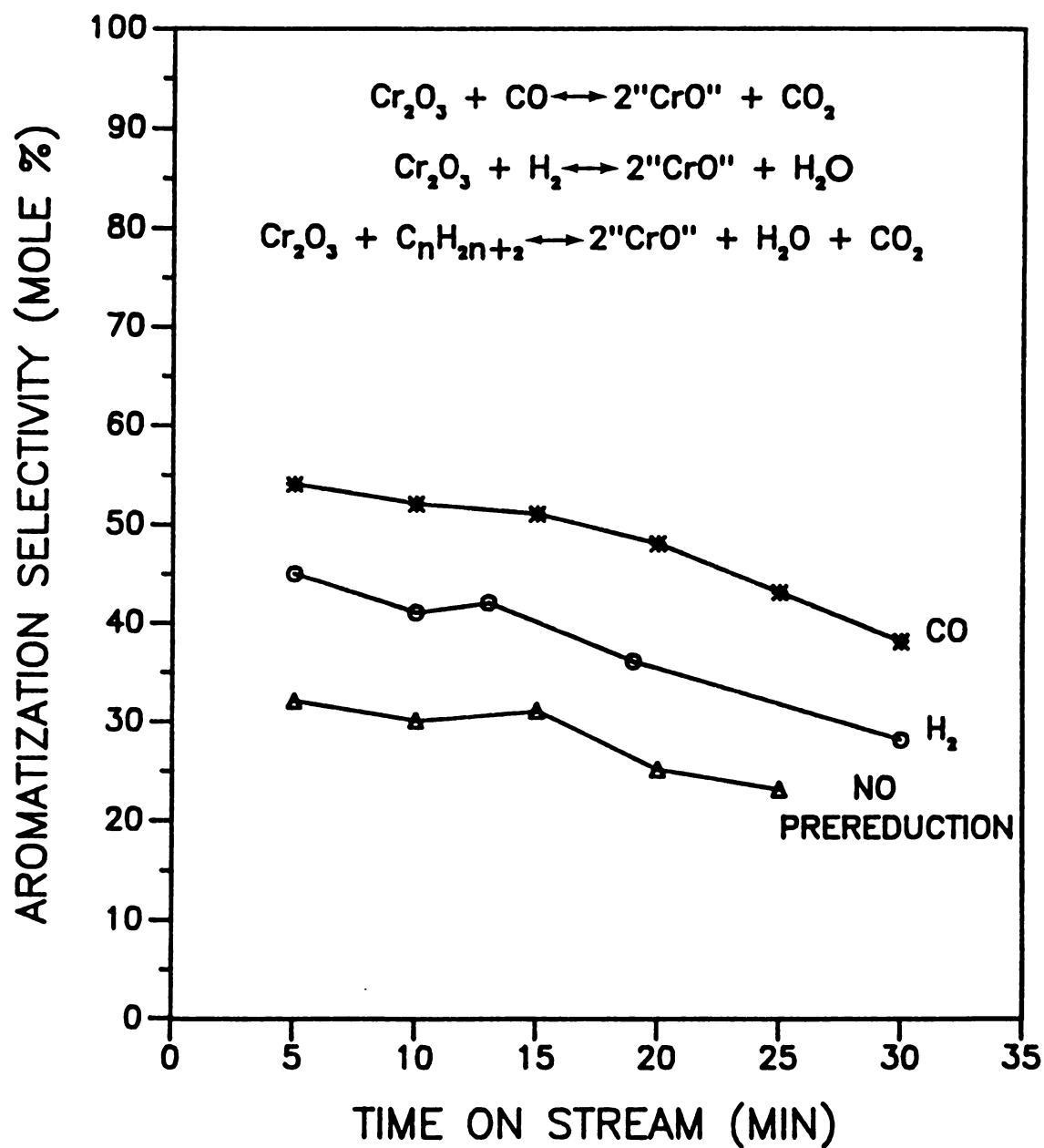


Figure 15. Octane aromatization selectivity versus time for DE-CPM catalyst with/without prereduction.

Table 9. Effect of catalyst prereduction on n-octane aromatization^(a).

Catalyst/ Reductant	Conv ^(b)	Arom Select.	Composition of Arom. Fraction ^(c)					
			Benz.	Tol.	E.B.	o-	m-	p-Xyl.
DE-CPM/ (None)	20	33	6.7	11.5	9.7	27.1	29.3	15.8
DE-CPM/ (Hyd)	23	45	4.9	7.3	16.3	36.7	22.3	12.5
DE-CPM/ (CO)	25	51	5.7	6.7	23.4	48.0	10.7	5.4
Reg CPM/ ^(e) (CO)	18	32	5.3	9.8	7.6	27.7	32.2	17.3
CPB/ (CO)	16	45	5.8	6.6	24.3	45.3	12.6	5.3
	Basal Spacing=16.5Å and Surface Area=254m ² /g							
CPF/ (CO)	12	20	6.8	4.1	35.6	41.4	8.3	3.8
	Basal Spacing=14.3Å and Surface Area=177m ² /g							
Cr/Alumina (None)	21	53	10.1	9.5	31.3	45.8	1.5	1.8
Cr/Alumina (CO)	11	66	6.9	6.5	36.3	47.1	1.3	2.0

(a) n-octane weight hourly space velocity = 2.5 hour⁻¹, reductant gas contact time = 1.5 sec for 2 hours, He carrier gas contact time = 1.5 sec., temperature = 500°C. All values are in mole percent after 5 min time one stream.

(b) Total conversion of n-octane to all products: cracked, isomerized, and aromatized.

(c) Composition of aromatic fraction: benzene, toluene, ethyl benzene, o-xylene, m-xylene, p-xylene.

volatilized the coke. The originally deactivated black catalyst was returned to its original green/blue color, then prereduced with carbon monoxide. The regenerated and prereduced catalyst showed similar conversion and selectivity to that of fresh DE-CPM without being prereduced. The regenerated catalyst also showed the highest para-xylene and the lowest ethyl benzene selectivity.

Carbon monoxide prereduced catalysts resulting from the chromia pillaring of the higher charge density smectites beidellite and fluorohectorite, CPB and CPF, with basal spacings of 16.5 and 14.3Å respectively, showed lower activity and aromatization selectivity than carbon monoxide prereduced DE-CPM.

The carbon monoxide prereduced chromia on alumina catalyst, when compared to non reduced chromia on alumina, showed increased, as well as the highest, aromatization selectivity, and decreased, as well as the lowest, conversion. This catalyst also showed the highest selectivity towards ethyl benzene and the lowest selectivity towards meta-xylene of all the catalysts tested.

Figure 16 depicts the decreasing selectivity towards o-xylene for the commercial chromia on alumina catalyst as it deactivates over time. However, the chromia pillared montmorillonite catalysts resulting from direct exchange or in-situ hydrolysis of the chromia pillaring solution show the opposite trend. The chromia pillared hectorite catalyst

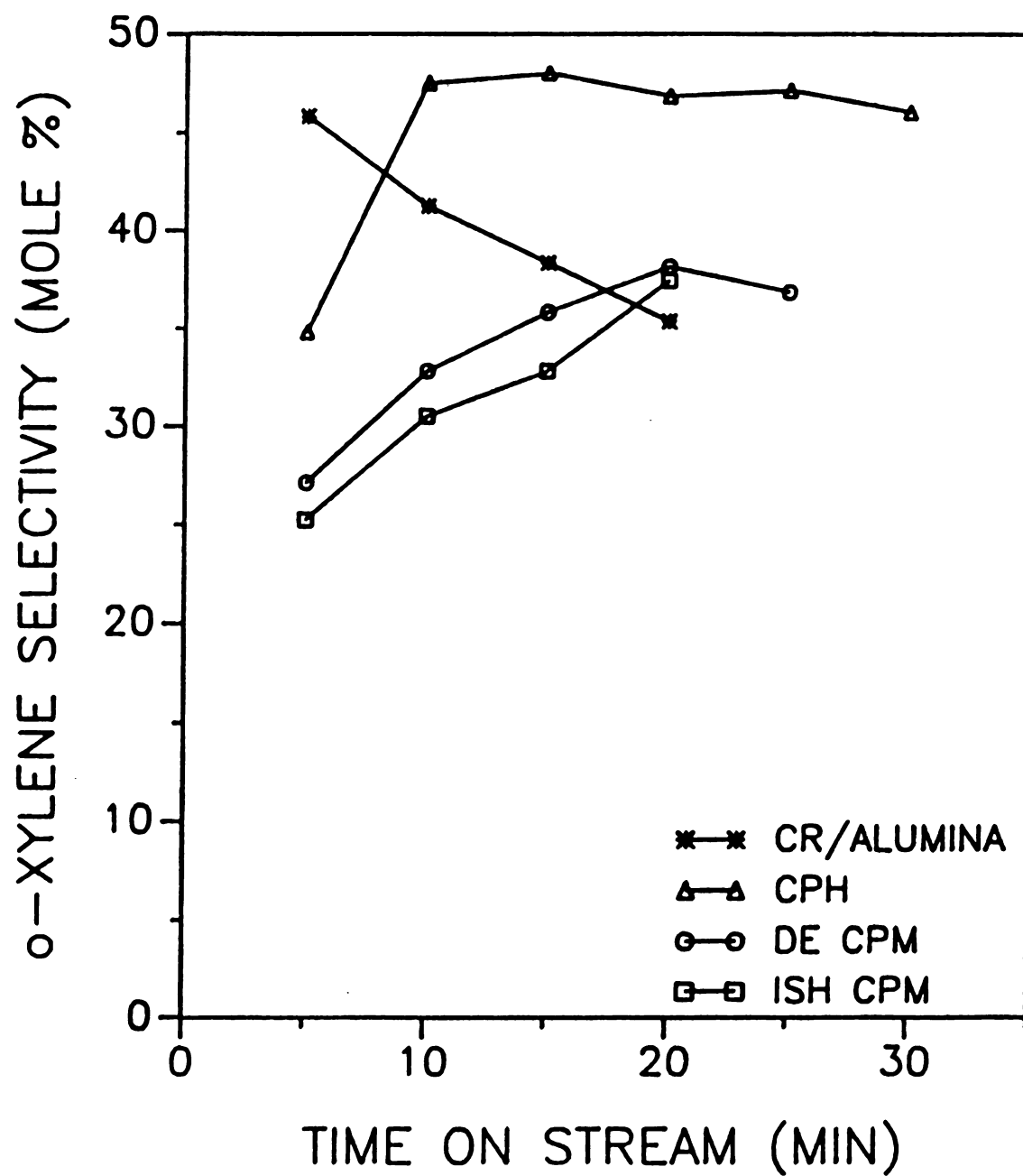


Figure 16. Octane aromatization selectivity to o-xylene with time over various chromia catalysts.

showed an initial increase in selectivity to o-xylene, which then became fairly constant over time.

Figures 17 and 18 show a similar trend for the decreasing selectivity to both meta- and para-xylene over time for the various chromia pillared clay catalysts. The CPH selectivity for m-xylene appears to initially diminish rapidly, then level off, while the chromia/alumina catalyst showed negligible selectivity for both meta- and para-xylene continually.

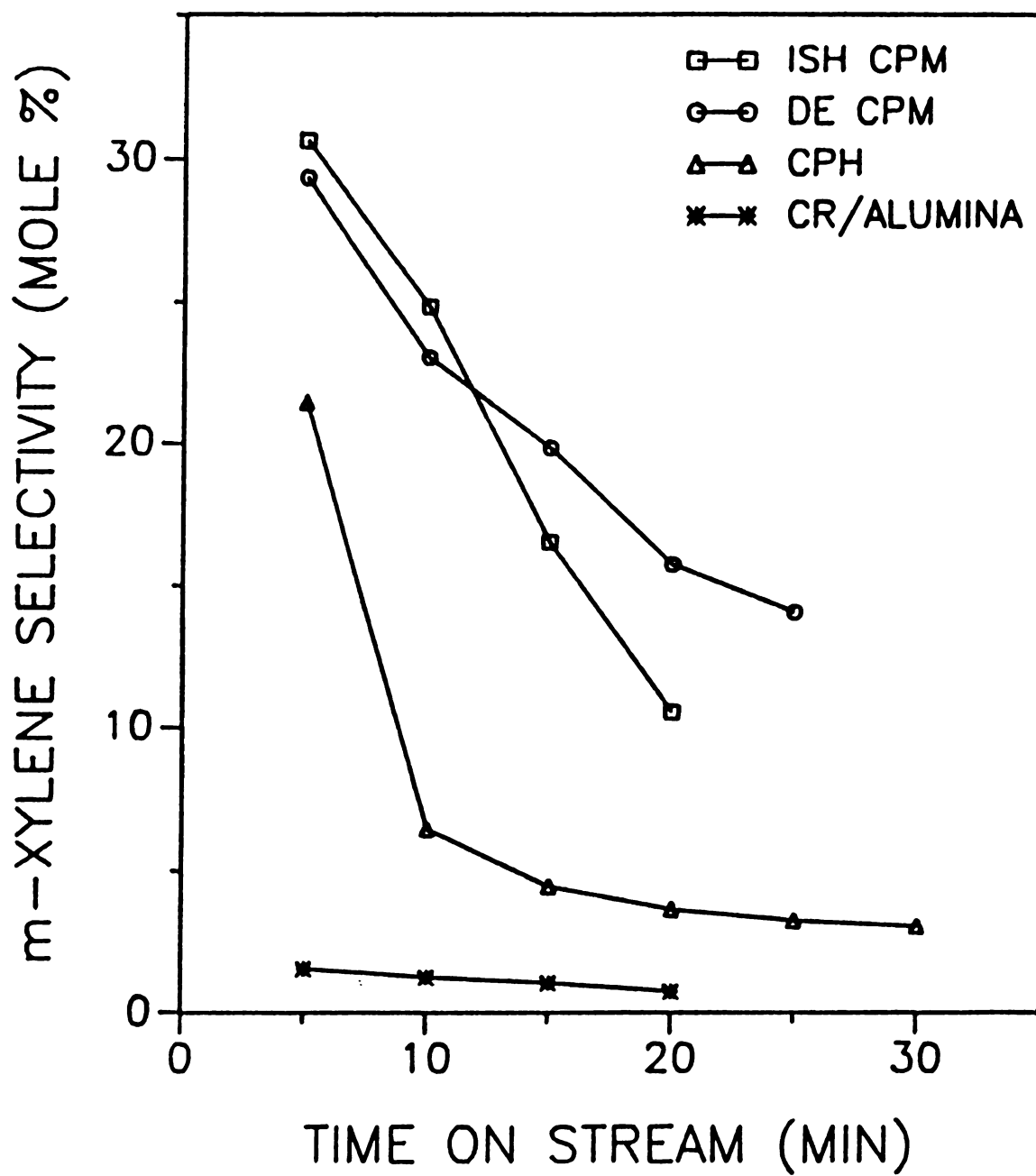


Figure 17. Octane aromatization selectivity to m-xylene with time over various chromia catalysts.

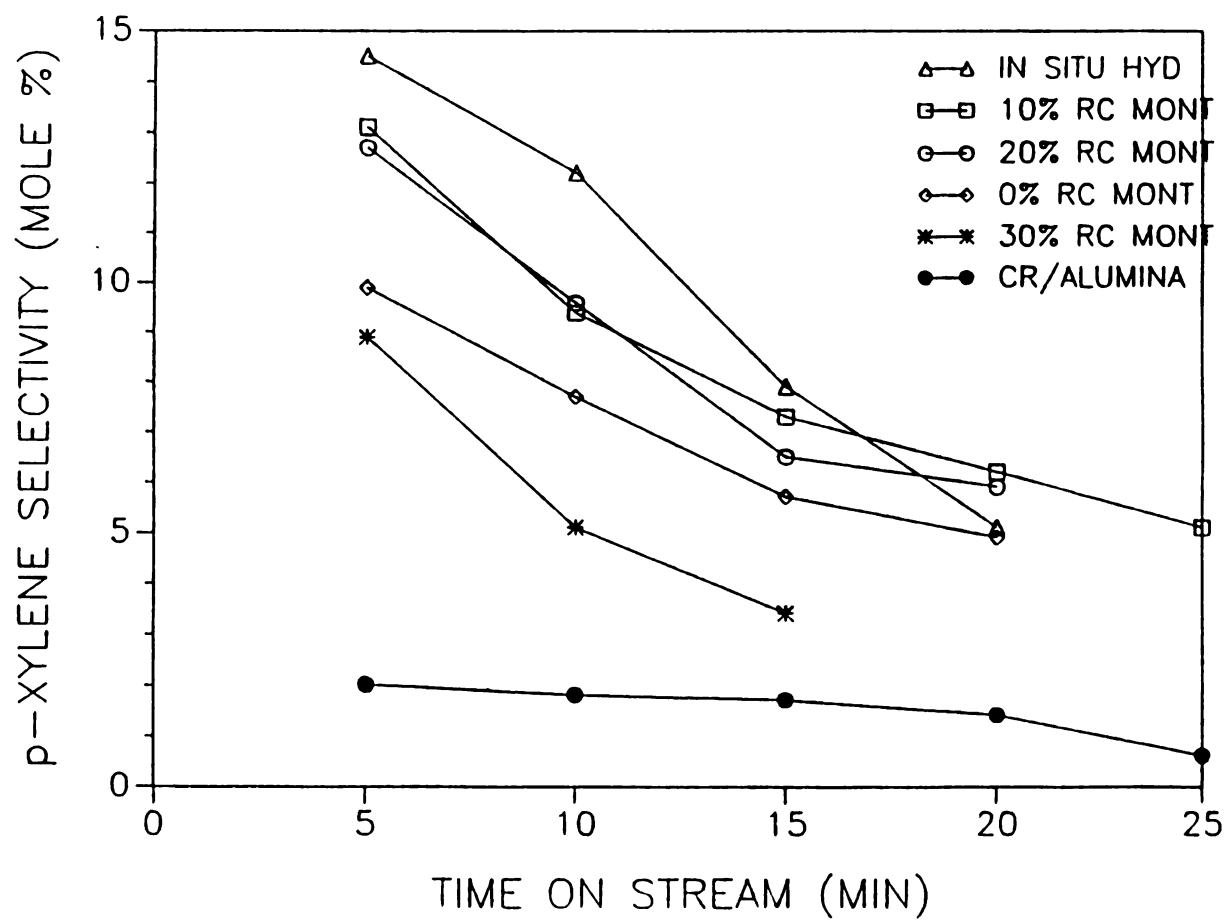


Figure 18. Octane aromatization selectivity to p-xylene with time over various chromia catalysts.

DISCUSSION

The presence of a larger number of Lewis acid sites than Bronsted acid sites in chromia pillared clays is consistent with the findings of Breen and coworkers (25), who studied the acidity of Cr^{3+} exchanged montmorillonite. They found that the Bronsted and Lewis acid sites were stable up to 200°C. In contrast, the chromia pillared montmorillonite acid sites in our study were stable at 300°C, as determined by pyridine adsorption. Also, these acid sites are available for catalytic reactions even at 500°C. It is likely that as the cationic pillars dehydrate, and dehydroxylate, Bronsted sites get converted to Lewis sites. However, there is still infrared evidence of Bronsted acidity at the elevated temperatures. Using the band assignments of Ward (25), it is difficult to conclude a replacement of Bronsted sites for Lewis, since the peaks tend to overlap. It is apparent from the pyridine bonding studies shown in Figures 2 and 3 that the total acidity (Bronsted and Lewis) of DE-CPM decreases rapidly with increasing temperature, and that physisorbed and hydrogen-bonded pyridine diminish at or below 100°C.

Even though the apparent acidity of a chromia pillared clay diminishes with increasing temperature, CPM and CPH are still able to act as solid acid catalysts for both a gas oil and n-decane cracking. The higher cracking activity observed for CPH over CPM is likely related to its larger

gallery height and higher surface area. However, the pores created by the chromia pillars appear to promote coking, which can be thought of as an extensive dehydrogenation product.

A common method of regenerating fouled catalysts is to thermally oxidize the contaminants in air. The problem with such an approach is that some or all of the catalytic sites can be affected by the thermal treatment, such as a change in their oxidation state. In this case, it appears that the catalytic sites responsible for cracking to hydrocarbons in the gasoline range become altered by the thermal oxidation of coke. Another explanation would be that acid strength decreases due to a weaker electrostatic potential created by pillar migration and decomposition, resulting in a decrease in microporosity. This would also explain the similar MAT conversion for both a fresh and regenerated DE-CPM (see Table 1). The number of acid sites in fresh and reactivated catalysts can be similar, yet the decreased acid strength caused by thermal activation of coke can limit cracking to above the gasoline range.

The low conversion, low gasoline selectivity, and minimal coking of the RTH-CPM indicate that the reduced gallery height, which results from intercalation of smaller chromium oligomeric cations, impedes accessibility of the reactants to the catalytic sites. This also shows that the catalytic sites of DE-CPM are located in the interlayer

space, since the outer surface of the clay layers are always accessible to the reactants.

The decane cracking product distributions in Table 7 can be explained based on competitive reaction pathways involving a nonclassical pentacoordinated carbonium ion mechanism and a classical catalytic cracking mechanism (26). Nonclassical pentacoordinated carbonium ions contain a carbon atom bound by three single bonds and one two-electron, three-center bond. The classical reaction mechanism in catalytic cracking includes β -scission, bimolecular hydrogen transfer, isomerization, and buildup (coking) reactions. β -scission is the only step in which a C-C bond is broken. Based on the stability rules for carbenium ions, C_2 hydrocarbons are disfavored relative to C_3 - C_6 hydrocarbons. Therefore, the classical mechanism seems to be favored for DE-CPM at 350°C, but not at 500°C, as judged from the relative abundance of C_2 versus higher carbon number production.

At the higher reaction temperature, the pentacoordinated carbonium ion mechanism appears to dominate due to a reduced sorption ability for hydrocarbons. There is therefore a lower probability for the bimolecular β -scission mechanism and increased production of C_2 hydrocarbons (27). In addition, increasing the temperature should favor the perturbing effect of the pillared clay pores on the reacting molecules, similar to that observed for zeolite pores (26). Molecules in pores can be activated

by the electrostatic field and the field gradient, which can weaken some C-C bonds. The pentacoordinated carbonium ion pathway is associated with the presence of high field gradients arising from small pores or polarizing cations. Smaller pores may be created at the higher reaction temperatures due to a decrease in the pillared clay basal spacing, and the chromia pillars can be considered as polarizing cations.

It has been shown that alumina can exert an effect on the acidic catalytic properties of chromia/alumina catalysts (28,29). The intrinsic acidic properties of alumina depend upon its method of preparation. The alumina used for this particular catalyst was of the "nonacidic" type. The low decane cracking conversion observed for the commercial chromia on alumina catalyst is a result of the low acidity of the alumina support. Therefore, the support interaction did not contribute to the cracking ability of the catalyst.

The low acidity of the alumina support may also increase the resistance of the chromia/alumina catalyst to deactivation by coking. Also, low coke formation would explain the high aromatization selectivity of chromia/alumina. Carbonaceous deposits are known to selectively inhibit dehydrocyclization reactions of paraffins which lead to 1,6 ring closure (30). A previous study on the dehydrocyclization of n-octane over a chromia/alumina/potassium oxide catalyst of low acidity revealed similarly high aromatic selectivity, with 94% of

the aromatic fraction being ethylbenzene and o-xylene, which are the only products of 1,6- and 2,7-ring closure of n-octane (31). This latter work also concluded that the dehydrocyclization activity of chromia/alumina catalysts decreases with time on stream. We also observed a similar loss of dehydrocyclization activity for chromia/alumina and for chromia pillared clays.

Chromia pillared clays consistently showed higher selectivity for m- and p- xylenes than Cr/alumina. These latter isomers are not believed to be isomerization products of either o-xylene or ethylbenzene over non-acidic oxide catalysts such as Cr/alumina (32). We already have noted the catalytic acidity of chromia pillared clays in cracking reactions. This acidity could either isomerize n-octane into branched-chain octanes before the aromatization reaction, or more likely, isomerize the products of n-octane aromatization.

It has been noted that deactivation of chromia/alumina catalysts does not proceed in a homogeneous manner. That is, certain catalytic sites deactivate more rapidly than others (32,33). Therefore, the mechanism of the dehydrocyclization reaction can vary over time for chromia/alumina, and also for chromia pillared clays. This is evident in the increasing selectivity towards o-xylene, yet decreasing selectivity towards m- and p-xylene for chromia pillared clays depicted in Figures 5-7. Yet, o-xylene is a result of 1,6 ring closure of n-octane, and

deactivation should minimize its formation similar to that observed for chromia/alumina.

The unique aromatic product distributions observed for chromia pillared clay catalysts compared to Cr/alumina can be explained by comparing the microenvironment of the aromatization reaction. For chromia/alumina, we are observing mainly a chromia catalyzed reaction with little or no complications caused by the alumina support. However, for the chromia pillared clays, the reaction occurs within acidic pores defined by chromia pillars of varying size and the upper and lower clay basal planes. The reactant molecule, once inside the pillared clay's porous network, is affected by the pore and adopts a conformation that maximizes its interaction with the walls. Pore effects are most commonly associated with zeolites, and are sometimes termed either "confinement effects" (34) or "the nest effect" (35). The diffusional behavior of reactants and products are regulated by the pore structure, and the molecules optimize their interaction with the environment by modifying their conformations.

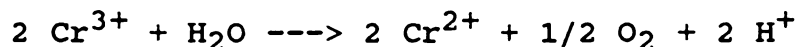
Pore effects on catalyst selectivity have also been explained based on collision theory and high-temperature physical adsorption theory, neither of which concerns the nature of the active catalytic sites (36). It has been concluded that a substantial increase in reaction rate and a change in selectivity will occur if the capillary size is reduced to a few molecular diameters. When the capillary or

pore size is reduced, physical adsorption will alter certain reaction rates to a much greater extent than if the pore size was large or nonexistent. In addition, the mean-free path for collision is reduced in a pore, which will result in increased activity.

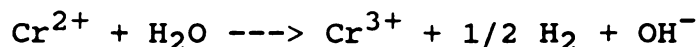
Porous supports are not a necessary requirement for high activity and selectivity in the aromatization reactions of n-paraffins. Recently, a novel aromatization catalyst, Pt-Mg(Al)O, was developed which was nonporous, yet exhibited similar catalytic properties as commercial zeolite catalysts for the conversion of n-hexane to benzene (37). Since there are no channels or pores in the magnesia support, there can be no stabilization of a cyclic intermediate due to the influence of spatial constraints. It is possible that the aromatization selectivity is determined by the electronic and atomic structure of the platinum clusters. Electronic effects could also explain our observations of higher aromatization selectivity for a commercial chromia/alumina catalyst relative to chromia pillared clays. That is, the electronic, and possibly the atomic, structure of chromia supported on alumina is different than that comprising the chromia pillars.

Currently, there is still no agreement as to the active oxidation state of chromium for various reactions. In this study, it appears that a reduced form of chromium, namely Cr^{2+} increases aromatization selectivity. However, as Figure 15 shows, hydrocarbons in the feed can be considered

as a reductant, which further complicates the oxidation state issue. In addition, the dehydration/dehydroxylation step in chromia pillared clay synthesis can partially reduce the Cr cations by oxidation of the liberated water (38):



This reaction would also generate Bronsted acidity. When either hydrogen or hydrocarbons are used as a reductant, the resulting water that is produced may hydrolyze the pillars and degrade them. Depending on temperature, the water may also interfere with chromium reduction by reduction of water:



The complicating effects of water may be eliminated using CO as a reductant, which may explain why carbon monoxide reduction resulted in the highest aromatization selectivity.

In general, aromatization activity and selectivity appear to be dependent on the type of chromia utilized. For chromia pillared clay, the nature of the chromia depends on the synthesis conditions and on the smectite host layer charge. Layer charge also has a pronounced effect on chromia pillared clay gallery heights (20), and therefore pore sizes, which influence the product distribution.

The mechanism for the catalytic aromatization of alkanes in the presence of chromia has been reviewed by Pines and Goetschel (28). They proposed a free-radical mechanism to explain the aromatization of alkanes over chromia/alumina catalysts. In their work they noted the

importance of the acidity of the alumina support. In our work with chromia pillared clays, the clay is serving essentially as a support, and the acidity of smectite clays may influence chromia pillared clay catalytic activity and selectivity.

Adsorbed transition state species resulting from the 1,7 and 1,8 ring closure of n-octane has been used to explain the formation of m- and p-xylene over Cr/alumina (39). This mechanism was developed to explain the selectivity of chromia/alumina catalysis. Such large cyclic molecules might also be accommodated in the pores of a chromia pillared clay. Pines and Nogueira concluded that three types of reactions participate during aromatization over chromia/alumina catalysts (40):

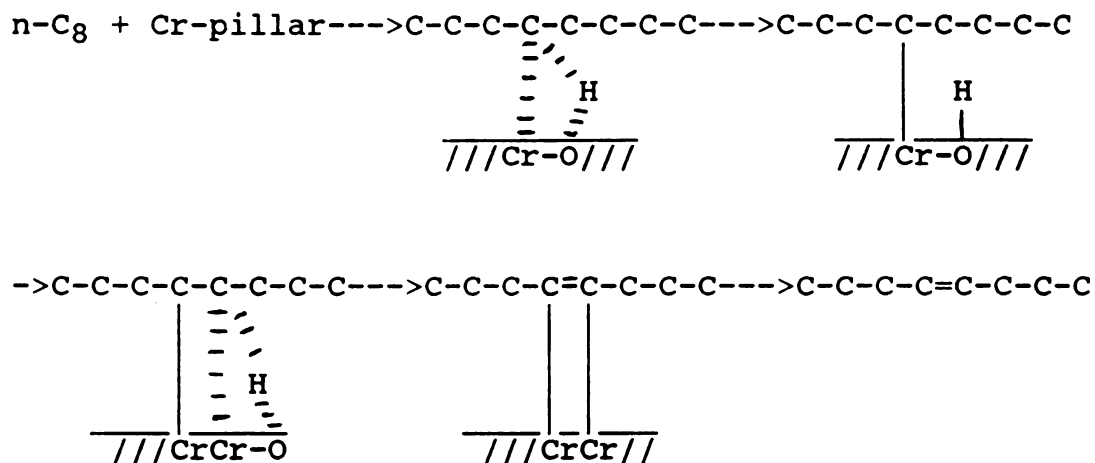
1. Catalytic dehydrogenation with the evolution of hydrogen.
2. Free-radical skeletal isomerization of the resulting alkenes followed by vinyl migration.
3. Thermal cyclization.

Therefore, the unique behavior of chromia catalysts in aromatization reactions can be attributed to a homolytic cleavage of an organometallic bond formed between chromium and carbon (41).

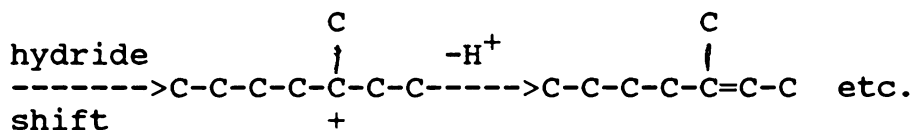
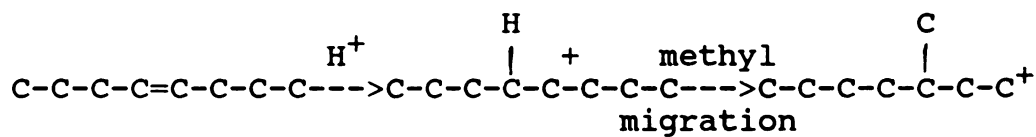
The above mechanism could also occur in the pillared clay galleries, however, because of their intrinsic acidity, the isomerization step could be acid catalyzed via a

carbonium ion. A proposed mechanism for the formation of p-xylene is:

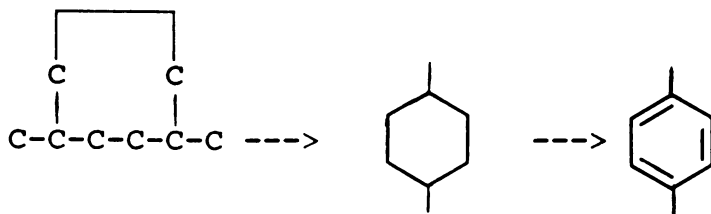
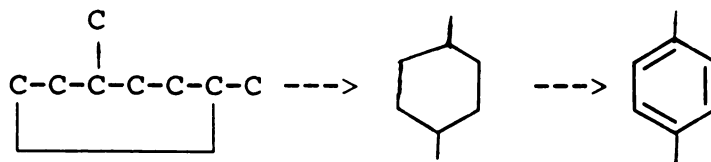
1. Dehydrogenation of n-octane to octene on chromia pillars.



2. Bronsted acid catalyzed skeletal isomerization of the alkene from step 1 or Lewis acid catalyzed abstraction of a hydride ion from n-octane. All that is necessary is a carbonium ion initiator.



3. 1,6-ring closure of 3-methylheptane or 2,5-dimethylhexane followed by dehydrogenation. These are the only isomers which will form p-xylene as a result of 1,6-ring closure.



While chromia pillared clay pores are too large to be completely shape selective for n-octane aromatization to p-xylene, the presence of acid sites, spatial constraints, and a unique and variable chromia species lead to an increase in selectivity to p-xylene.

REFERENCES

1. Weisz, P.B. and Frilette, V.J. J. Phys. Chem. **1960**, 64, 382.
2. Derouane, E.G. in Zeolites: Science and Technology, **1984**, F.R. Ribeiro, A.E. Rodrigues, L.D. Rollmann, and C. Naccache, eds., Martinus Nijhoff Publishers: The Hague, 347-371.
3. Csicsery, S.M. Zeolites **1984**, 4, 202.
4. Chen, N.Y. in Perspectives in Molecular Sieve Science, ACS Symposium Series 368, **1988**, W.H. Flank and T.E. Whyte, Jr., eds., American Chemical Society: Washington, DC, 468-477.
5. Ballantine, J.A. in Chemical Reactions in Organic and Inorganic Constrained Systems, **1986**, R. Setton, ed., D. Reidel Publishing Company, 197-212.
6. Sterte, J. in Symposium On New Catalytic Materials And Techniques Presented Before The Division Of Petroleum Chemistry, Inc., chapter 10, **1990**, American Chemical Society: Washington, DC, 489-496.
7. Tichit, D.; Fajula, F.; Figueras, F.; Gueguen, C.; Bousquet, J. 112-119.
8. Guan, J.; Min, E.; Yu, Z. in Proceedings 9th International Congress on Catalysis, **1988**, M.J. Phillips and M. Ternan, eds., Ottawa, Ontario, 104.
9. Occelli, M.L.; Landau, S.D.; Pinnavaia, T.J. J. Catal. **1987**, 104, 331.
10. Wenyang, X.; Yizhao, Y.; Xianmei, X.; Shizheng, L.; Taoying, Z. Appl. Catal. **1991**, 75, 33.
11. Raythatha, R.H. U.S. Patent 4,855,268, **1989**.
12. Schutz, A.; Plee, D.; Borg, F.; Jacobs, P.; Poncelet, G.; Fripiat, J.J. in Proceedings of the International Clay Conference, Denver, 1985, **1987**, L.G. Schultz, H. van Olphen, and F.A. Mumpton, eds., The Clay Minerals Society: Bloomington, Indiana, 305-310.
13. Vaughan, D.E.W. in Perspectives in Molecular Sieve Science, ACS Symposium Series 368, **1988**, W.H. Flank and T.E. Whyte, Jr., eds., American Chemical Society: Washington, DC, 308-323.

14. Gutierrez, E. and Ruiz-Hitzky, E. Pillared Layered Struct.: Curr. Trends Appl., [Proc. Workshop], 1990, I.V. Mitchell, ed., Elsevier: London, UK, 199-208.
15. Suzuki, K. and Mori, T. J. Chem. Soc., Chem. Commun. 1989, 7.
16. Horio, M.; Suzuki, K.; Masuda, H.; Mori, T. Appl. Catal. 1991, 72, 109.
17. Mori, T. and Suzuki, K. Chemistry Letters 1989, 2165.
18. Burwell, R.L. Jr.; Haller, G.L.; Taylor, K.C.; Read, J.F. in Advances in Catalysis and Related Subjects, 1969, 20, D.D. Eley, H. Pines, and P.B. Weisz, eds., Academic Press: New York, 1-96.
19. Choudary, B.M.; Durgaprasad, A.; Valli, V.L.K. Tetrahedron Lett. 1990, 31, 5785.
20. Brewer, T.D. and Pinnavaia, T.J., in press.
21. Brindley, G.W. and Ertem, G. Clays Clay Miner. 1971, 19, 399.
22. Pinnavaia, T.J.; Tzou, M.S.; Landau, S.D.; Raythatha, R.H. J. Molec. Catal. 1984, 27, 195.
23. Ward, J.W. J. Colloid Interface Sci. 1968, 28, 269.
24. Tichit, D.; Fajula, F.; Figueras, F.; Gueguen, C.; Bosquet, J. in Fluid Catalytic Cracking: Role in Modern Refining, ACS Symposium Series 375, 1988, Mario L. Occelli, ed., American Chemical Society: Washington, D.C., 237-252.
25. Breen, C.; Deane, A.T.; Flynn, J.J. Clay Miner. 1987, 22, 169.
26. Mirodatos, C. and Barthomeuf, D. J. Catal. 1988, 114, 121.
27. Haag, W.O. and Dessau, R.M. in Proceedings 8th International Congress on Catalysis, Vol. II, 1984, Verlag Chemie, Weinheim, 305.
28. Pines, H. and Goetschel, C.T. J. Org. Chem. 1965, 30, 3530.
29. Pines, H. and Haag, W.O. J. Am. Chem. Soc. 1960, 82, 2471.
30. Horsley, J. in Catalytica Highlights 1991, 17(2), 1.



31. Hassan, S.M.; Abdou, I.K.; Roushdi, M.I.; Elkadi, G.M. J. Chem. Tech. Biotechnol. **1981**, 31, 751.
32. Pines, H. and Chen, C.T. J. Am. Chem. Soc. **1960**, 82, 3562.
33. Pines, H. and Chen, C.T. J. Org. Chem. **1961**, 26, 1057.
34. Derouane, E.G.; Nagy, J.B.; Fernandez, C.; Gabelica, Z.; Laurent, E.; Maljean, P. Appl. Catal. **1988**, 40, L1-L10.
35. Derouane, E.G. J. Catal. **1986**, 100, 541.
36. Freeman, M.P. J. Colloid Interface Sci. **1971**, 37, 760.
37. Davis, R.J. and Derouane, E.G. Nature **1991**, 349, 313.
38. Cornet, D. and Chambellan, A. in Catalysis by Acids and Bases, Studies in Surface Science and Catalysis 20, **1985**, B. Imelik, C. Naccache, G. Coudurier, Y. Ben Taarit, J.C. Vedrine, eds., Elsevier, Amsterdam, 273-282.
39. Pines, H.; Goetschel, C.T.; Csicsery, S.M. J. Org. Chem. **1963**, 28, 2713.
40. Pines, H. and Nogueira, L. J. Catal. **1981**, 70, 391.
41. Pines, H. J. Catal. **1982**, 78, 1.

CHAPTER IV
CHROMIA AND ALUMINA PILLARED MONTMORILLONITE
CATALYZED HYDROCONVERSION OF N-HEPTANE

INTRODUCTION

The potential of metal oxide pillared clays for the cracking of heavy feedstocks (1-4) as well as for hydrocracking-hydroisomerization (5,6) has recently been studied and compared to commercial zeolite catalysts. In general, pillared clays are comparable to zeolite catalysts except for having a higher coke yield and showing greater deactivation after steaming. However, an alumina pillared beidellite showed higher hydroisomerization selectivity than both an ultrastable zeolite Y catalyst and an alumina pillared montmorillonite catalyst(5). This high isomerization selectivity of alumina pillared beidellite can be attributed to both its larger pore size than zeolites and its higher acidity than alumina pillared montmorillonite(5,6).

Transition metal oxide pillared clays are of particular interest in that they should show enhanced cracking selectivity due to the inherent acid cracking catalytic activity of many transition metal species(7). Chromia is



one such species, and a chromia interlayered montmorillonite clay was first synthesized by Brindley and Yamanaka in 1979, utilizing the base catalyzed hydrolysis of chromium cations at room temperature(8). Subsequent improvements in the synthesis conditions has resulted in larger gallery height materials, with the final chromia pillared montmorillonite containing catalytically active chromia pillars for the dehydrogenation of cyclohexane to benzene (9,10).

The siting of chromium in alumina pillared clay has been shown to have substantial catalytic consequences. Jacobs and co-workers (11) found chromium to have a beneficial effect on the activity of a catalyst, composed of 1 wt% platinum exchanged on a clay interlayered by an (Al + Cr) solution, for the isomerization of n-decane. In addition, Suib, Coughlin and co-workers (12) prepared pillared clays in which chromium was either doped into the alumina pillar or resided on the gallery surfaces between the alumina pillars. Both Cr/Al pillared clays exhibited higher activity than alumina pillared clay for the hydrocracking of n-decane, while producing less coke.

This paper compares the activity and isomerization selectivity of chromia pillared montmorillonite (CPM) and alumina pillared montmorillonite (APM) catalysts for the hydroconversion of n-heptane.

EXPERIMENTAL

Chromia Pillared Montmorillonite

Chromium polyoxocations were synthesized by hydrolysis of chromium nitrate at a base to Cr ratio of 2.0 (equiv/mol). A 300-ml portion of 0.17M chromium nitrate (50 mmol) and 200-ml aliquot of 0.25M sodium carbonate (50 mmol) were freshly prepared for use in pillaring one gram (0.80 meq) of Na^+ -montmorillonite clay. The sodium carbonate solution was transferred into the vigorously stirring chromium nitrate solution at a rate of 10 ml/min. The resulting solution was then heated to 95°C and aged at this temperature for 36 hours.

A 1.0 wt% suspension of purified Na-montmorillonite was added dropwise to the warm hydrolyzed chromium solution, and the mixture was stirred for 1.5 hours. The exchanged clay was collected by centrifugation, washed free of excess salt by repeated centrifugation/dispersion cycles, and dried in air by evaporating a 1.0 wt% suspension on glass sheets. The product is then dehydrated/dehydroxylated at 350°C for 2 hours under Ar. A heating rate of 5°C/min was used to achieve the drying temperature.

Alumina Pillared Montmorillonite

A previously published procedure was used for the preparation of alumina pillared montmorillonite (13). A

hydroxy-aluminum solution with a OH/Al ratio of 2.0 was prepared by adding 0.5M NaOH to 0.2M $\text{AlCl}_3 \cdot 6\text{H}_2\text{O}$ under stirring. The final solution was made 0.1M in Al by the addition of distilled water.

The hydrolyzed aluminum solution was then added to a Wyoming montmorillonite clay suspension until 30 meq Al/g clay was introduced. The mixture was allowed to stand for 30 min, after which it was dialyzed against distilled water until free of excess ions, and freeze-dried.

Physical Methods

XRD patterns were obtained with a Philips diffractometer using CuK alpha radiation and Ni-filters. CPM was analyzed as an oriented film, air dried from a 1 wt% aqueous suspension onto a glass slide. APM was analyzed as a powder.

Nitrogen adsorption-desorption isotherms (from which BET surface areas and porosities were obtained) were measured at liquid N_2 temperature, using ultra high purity N_2 gas. CPM samples were outgassed at 350°C under vacuum, then analyzed on a Quantasorb Autosorb sorption analyzer. APM samples were outgassed at 400°C under vacuum and analyzed in a conventional glass volumetric apparatus provided with Bell & Howell pressure gauges.

Chemical analysis was performed on a Jarrell Ash Atom Comp atomic absorption spectrometer. Samples were prepared using a lithium borate fusion technique at 1000°C.

N-heptane hydroconversion was performed in a fixed-bed continuous flow reactor operated at atmospheric pressure, with the carrier gas (He, H_2) flowing through a saturator kept at constant temperature. The hydrogen/hydrocarbon molar ratio was 16, and the weight hourly space velocity (WHSV) was 0.9 g n-heptane/g catalyst/hour. Both pillared clays were impregnated with a Pt (II) tetrammine complex to give a loading corresponding to 1 wt% of platinum metal. After being dried at 110°C , the catalyst powder was compressed, crushed, and sieved. 200 mg of the 0.3-0.6 mm fraction was loaded into the reactor between two layers of pure fine-grained quartz (0.2mm). The catalyst was activated by in-situ calcination at either 250°C or 400°C in air for 2 hours to form platinum oxide, and then the oxide was reduced in H_2 at the same temperature. The hydroconversion of n-heptane was carried out under temperature-programmed conditions, using a heating rate of $2^\circ\text{C}/\text{min}$. Effluent analysis was performed using a monitored 6-way sampling valve coupled with a HP5880 gas chromatograph with a high resolution capillary column.

RESULTS AND DISCUSSION

Physical Characterization

The final Cr or Al content that is intercalated as hydroxy-metal species within the gallery region is very similar for both pillared clays. APM contained 2.5 moles of intercalated Al per $O_{20}(OH)_4$ unit, while CPM contained 2.3 moles of intercalated Cr per unit cell.

The $d(001)$ basal spacings of APM and CPM were determined from their corresponding XRD patterns. CPM has over a 5\AA larger gallery height than APM, along with a larger BET surface area and a similar total pore volume (Table 10). These physical differences between APM and CPM can be explained by a more rod-shaped chromia pillar than that of alumina. This results in both a larger gallery height and less clay basal surface being covered by pillaring species. Both clays maintained their crystallinity after each catalytic run.

The acidity present in both APM and CPM has been determined previously and found to consist mainly of the Lewis type (5,14). Both clay catalysts also contained a small amount of Bronsted acidity.

Hydroconversion of n-heptane

Figure 19 shows the evolution of conversion vs reaction temperature for CPM activated at 400°C , while Figure 20



Table 10. Physical properties of APM and CPM

Sample	d(001) (a) (Å)	Surface Area (m ² /g)	Total Pore Volume (cm ³ /g)
APM (b)	17.8	250	0.21
CPM	23.2	289	0.21

(a): APM was dehydrated/dehydroxylated at 300°C under inert gas. CPM was dehydrated/dehydroxylated at 350°C under inert gas.

(b): From reference 6.



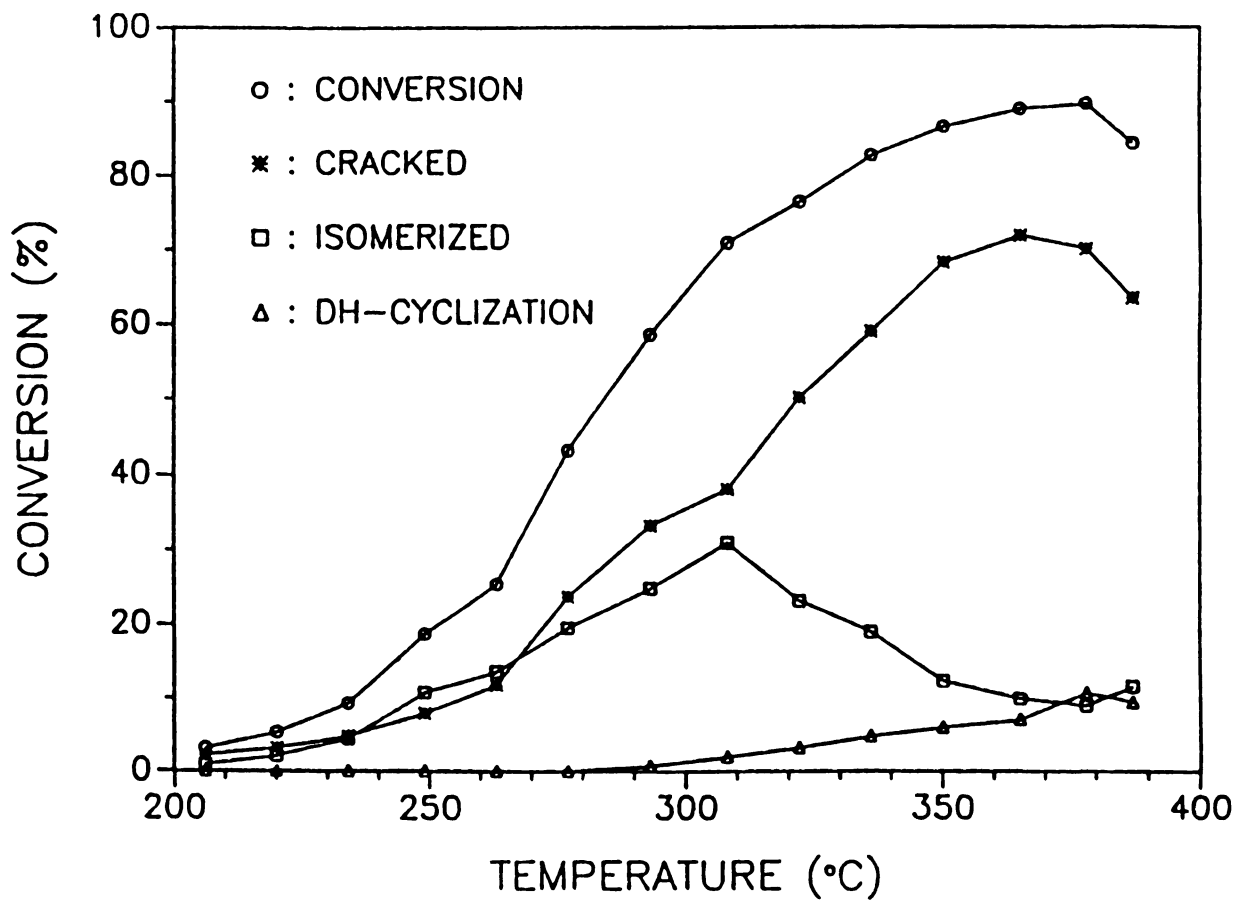


Figure 19. Temperature-programmed hydroconversion of n-heptane over CPM. Catalyst pretreatment: 2 hrs at 400°C in air, H₂.



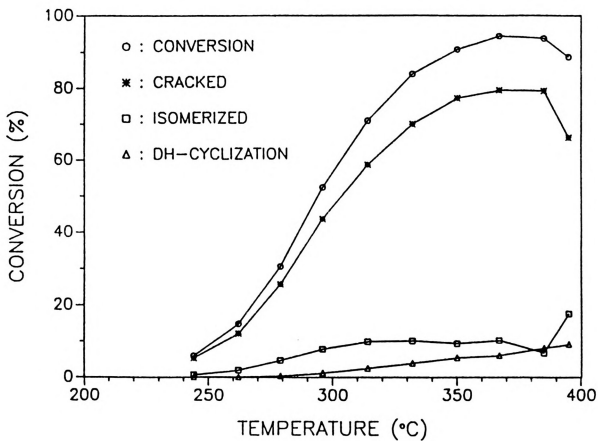


Figure 20. Temperature-programmed hydroconversion of n-heptane over CPM. Catalyst pretreatment: 2 hrs at 250°C in air, H_2 .



shows the results after activation at 250°C. The total conversion is similar for both pretreatment conditions, however, the selectivities for isomerization products vs cracked products varies with the activation temperature. CPM activated at 400°C shows a much higher isomerization selectivity than CPM activated at 250°C, indicating that the acid function is out of balance with respect to the metal function at the lower activation temperature. The increased isomerization activity associated with the higher activation temperature is most probably due to a decrease in chromia pillar acidity. The acid function is actually dominant for both pretreatment conditions, and cracked products parallel the total conversion. Therefore, the majority of the conversion products of CPM catalyzed hydroconversion of n-heptane is due to cracking. This can be expected since chromia is a known cracking catalyst.

The percent total hydroconversion of n-heptane for APM and CPM catalysts under temperature programmed conditions is compared in Figure 21. Both catalysts were activated at 400°C. The CPM catalyst results in slightly higher conversion levels, and is therefore more active, yet the APM catalyst shows a much higher selectivity for isomerized products, as shown in Figure 22. One would initially expect the larger pores present in CPM not to favor hydrogenolysis, since larger isomerized products could more easily diffuse out of a CPM gallery than an APM gallery. However, heptane and its isomers are not bulky enough molecules to yield

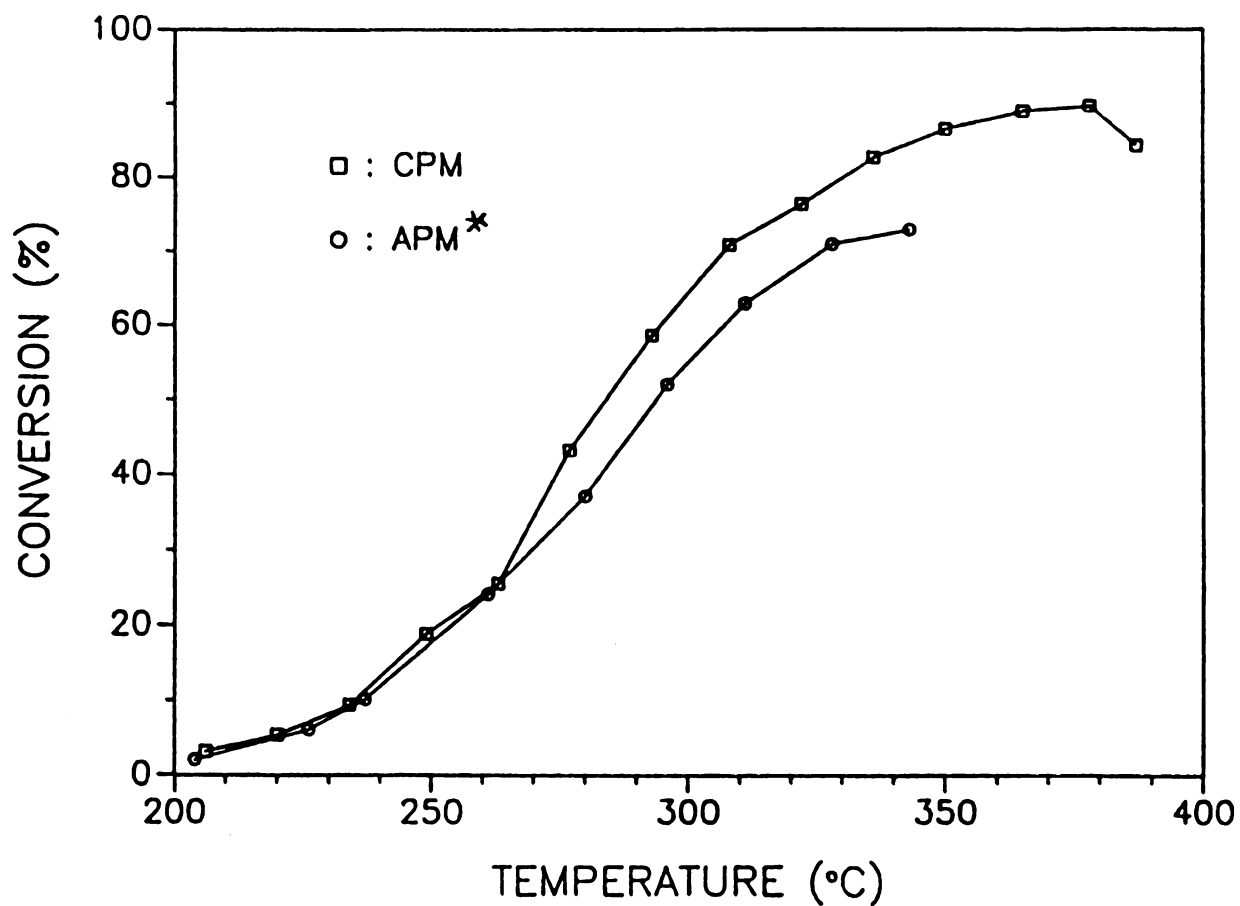


Figure 21. Temperature-programmed hydroconversion of n-heptane over CPM and APM. * (obtained from reference 6)

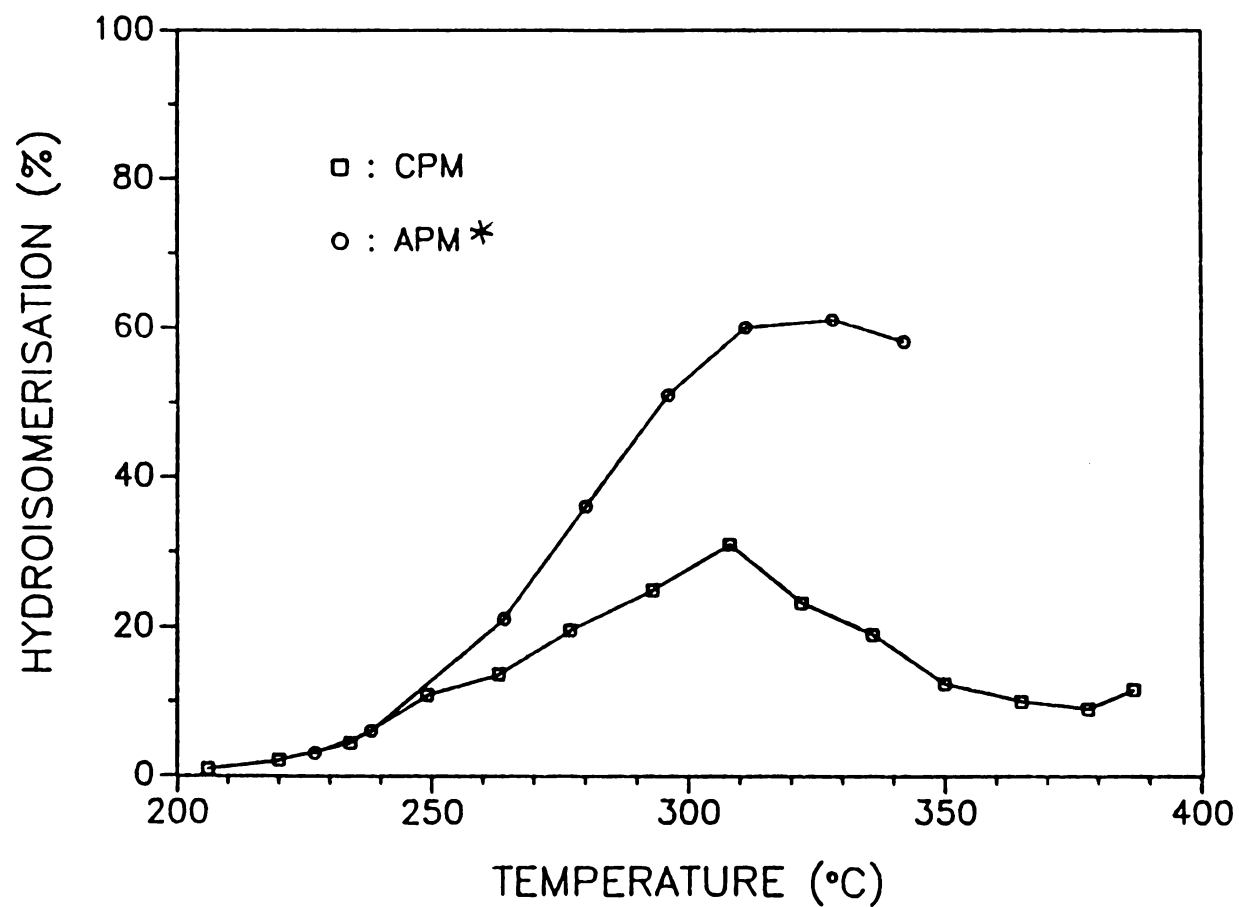


Figure 22. Percentage of C₇ isomers in the reaction products as a function of reaction temperature for the temperature-programmed hydroconversion of n-heptane over CPM and APM. * (obtained from reference 6)

information comparing pore shape and size since the products can diffuse freely in the intracrystalline pore volume of each pillared clay. In addition, chromia is a dehydrogenation catalyst, and a higher concentration of olefins favors coking, similar to the effect of Fe_2O_3 (15). Poncelet and Schutz (6) believe that H_3O^+ is the main source of acidity for APM, and upon dehydration at elevated temperatures, the protons migrate to the octahedral layer, where they are not available as catalytic acid sites. Therefore, the lower acidity of APM makes it a better hydroisomerization catalyst than CPM, while CPM is the better hydrocracking catalyst due to the dehydrogenation function present in chromia.

REFERENCES

1. M. Tokarz and J. Shabtai *Clays Clay Miner.*, 33, 89 (1985).
2. J. Shabtai, R. Lazar, and A.G. Oblad New Horizons in Catalysis, 7, 828-840 (1981).
3. R.J. Lussier, J.S. Magee, and D.E.W. Vaughan 7th Canadian Symp. Catal. 112 (1980).
4. M.L. Occelli Ind. Eng. Chem. Prod. Res. Devel., 22, 553 (1983).
5. A. Schutz, D. Plee, F. Borg, P. Jacobs, G. Poncelet, and J.J. Fripiat (1985).
6. G. Poncelet and A. Schutz in Chemical Reactions in Organic and Inorganic Constrained Systems, Ed. R. Setton, Reidel, 165-178 (1986).
7. L.L. Murrell, D.C. Grenoble, C.J. Kim, and N.C. Dispenziere, Jr. *Journal of Catalysis*, 107, 463 (1987).
8. G.W. Brindley and S. Yamanaka *Amer. Mineral.*, 64, 830 (1979).
9. T.J. Pinnavaia, M.S. Tzou, and S.D. Landau *J. Amer. Chem. Soc.*, 107, 2783 (1985).
10. M.S. Tzou and T.J. Pinnavaia *Catalysis Today*, 2, 318 (1988).
11. P. Jacobs, G. Poncelet, and A. Schutz French Patent 2512043 (1982).
12. K.A. Carrado, S.L. Suib, N.D. Skoularikis, R.W. Coughlin *Inorg. Chem.*, 25, 4217 (1986).
13. D. Plee, L. Gatinneau, and J.J. Fripiat *Clays Clay Miner.*, 35(2), 81 (1987).
14. M.S. Tzou Dissertation, Michigan State University (1983).
15. D. Tichit, F. Fajula, F. Figueras, C. Gueguen, and J. Bosquet Fluid Catalytic Cracking Role In Modern Refining, Ed. M.L. Occelli, ACS Symposium Series 375, Washington D.C. (1988).

MICHIGAN STATE UNIV. LIBRARIES



31293007929205